The launching of jets from astrophysical accretion disks and black holes

Ioannis Contopoulos

2nd HELAS Summer School, Athens July 14, 2016

- M87 jet: Curtis 1918
- Quasars: 60s
- Lynden-Bell 1969: Galactic nuclei as collapsed old quasars
- Lovelace 1976: Dynamo model of double radio sources
- Blandford 1976: Accretion disk electrodynamics

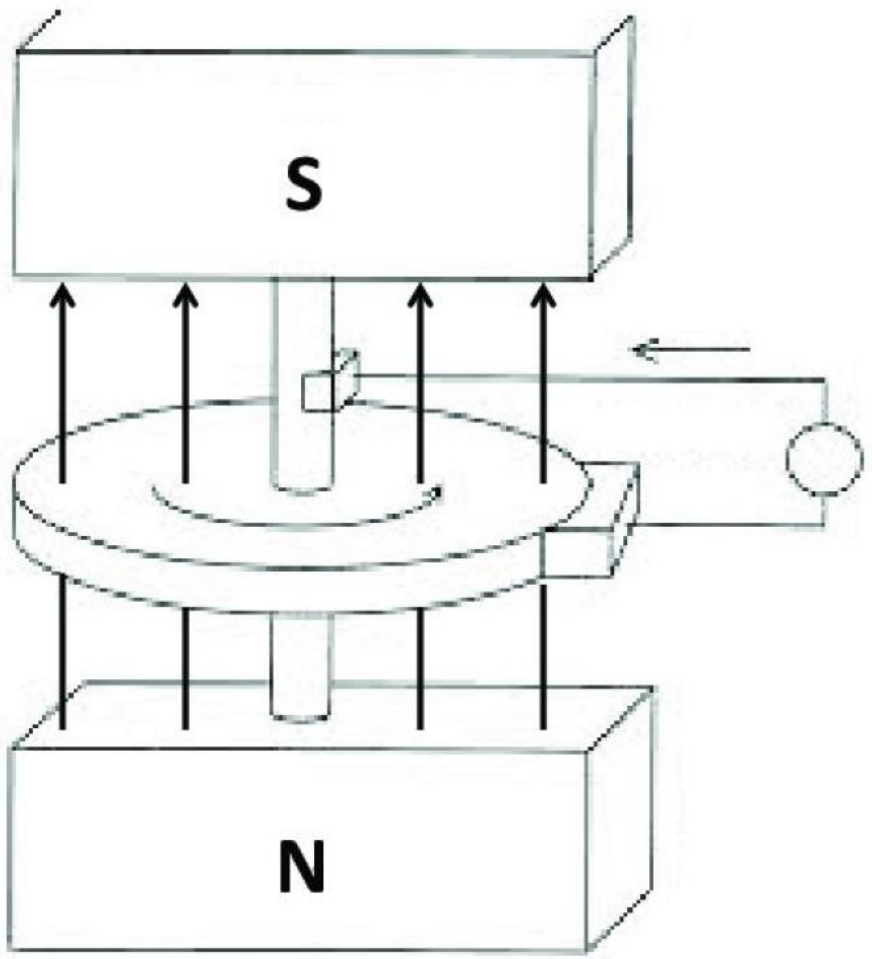

Figure 6. Faraday disk with conducting path and load that allow it to spin down exponentially. Vertical arrows: magnetic field.

The Faraday disk dynamo

$$\dot{E} \approx -\frac{1}{6\pi c}\Psi_{\rm m}^2\Omega^2 \approx 10^{44} \ \ {\rm erg/s}$$

$$E_{\rm max\ rot} = 29\% Mc^2 \approx 5\times 10^{62} M_9 \ \ {\rm erg}$$

The launching of MHD jets from astrophysical accretion disks

- “Hydromagnetic flows from accretion discs and the production of radio jets”, Blandford & Payne 1982
- “Magnetically driven jets and winds: Exact solutions”, Contopoulos & Lovelace 1994
- “A simple type of magnetically driven jets: an astrophysical plasma gun”, Contopoulos 1995
- “Magnetized accretion-ejection structures”, Ferreira & Pelletier 1993- and “Magnetohydrodynamic disk-wind connection”, Li Zhi-Yun 1995-96
- “The universal magnetic structure of black hole accretion disk winds”, Fukumura et al. 2016

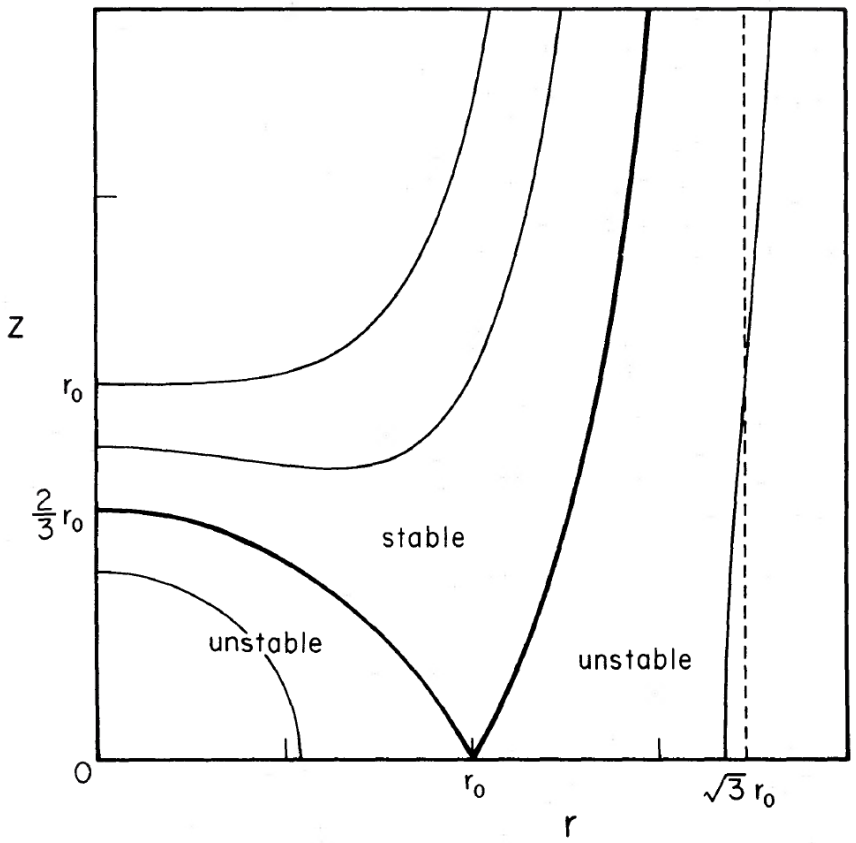

Figure 1. Equipotential surfaces for a bead on a wire, corotating with the Keplerian angular velocity $(GM/r_0^3)^{1/2}$ at a radius r_0, which is released from rest at r_0. The equation of the surfaces is

$$\phi(r,z) = -\frac{GM}{r_0}\left[\tfrac{1}{2}\left(\frac{r}{r_0}\right)^2 + \frac{r_0}{(r^2+z^2)^{1/2}}\right] = \text{constant}.$$

"Hydromagnetic flows from accretion discs and the production of radio jets", Blandford & Payne 1982

2.1 MHD EQUATIONS

The equations of stationary, axisymmetric MHD flow in cylindrical co-ordinates (r, ϕ, z) have been written down by several authors (e.g. Chandrasekhar 1956; Mestel 1961). The fluid velocity $\mathbf{v}(\mathbf{r})$ is related to the field strength $\mathbf{B}(\mathbf{r})$ by

$$\mathbf{v} = \frac{k\mathbf{B}}{4\pi\rho} + (\boldsymbol{\omega} \times \mathbf{r}), \tag{2.1}$$

where the undetermined constant $k/4\pi$ (which can be interpreted as the ratio of the constant mass flux to the constant magnetic flux) and the angular velocity ω satisfy

$$(\mathbf{B} \cdot \nabla)\, k = (\mathbf{B} \cdot \nabla)\, \omega = 0.$$

There are two constants of the motion, the specific energy

$$e = \tfrac{1}{2}v^2 + h + \Phi - \frac{\omega r B_\phi}{k}, \tag{2.2}$$

and the specific angular momentum

$$l = r v_\phi - \frac{r B_\phi}{k}; \tag{2.3}$$

that is, $$(\mathbf{B} \cdot \nabla)\, e = (\mathbf{B} \cdot \nabla)\, l = 0.$$

The gas density is obtained from the continuity equation,

$$\nabla \cdot (\rho \mathbf{v}) = 0. \tag{2.4}$$

Finally, we need the z-component of the momentum equation

$$\rho (\mathbf{v} \cdot \nabla)\, v_z = -\frac{\partial p}{\partial z} - \frac{\rho \partial \Phi}{\partial z} - \frac{1}{8\pi}\frac{\partial B^2}{\partial z} + \frac{1}{4\pi}(\mathbf{B} \cdot \nabla) B_z, \tag{2.5}$$

2.2 SELF-SIMILAR SOLUTIONS

As described in the introduction, we seek a self-similar solution for axisymmetric flow from an accretion disc in Keplerian orbit about a black hole of mass M, with $B(r, \phi, 0) \propto r^{-5/4}$. For the field lines meeting the disc at radius r_0, we introduce the scaling

$$\mathbf{r} = [r_0 \xi(\chi), \quad \phi, \quad r_0 \chi] \tag{2.6a}$$

$$\mathbf{v} = [\xi'(\chi) f(\chi), \quad g(\chi), \quad f(\chi)] \left(\frac{GM}{r_0}\right)^{1/2}, \tag{2.6b}$$

so that all quantities will scale with spherical radius along a given direction. In equations

to obtain a second-order differential equation for $\xi(\chi)$,

$$\begin{aligned} &\xi f^2 T (m-1)^2 (t-1)\, \xi'' + JS^2 \{(m-1)^2 [\xi T + (n-m-1) f^2 J]\, T \\ &\quad + m(m-1) [(t-1)\, \xi T S - \xi f^2 (\chi + \xi\xi')(\xi\xi' - \xi\xi' S^3 - \chi S^3)] \\ &\quad + (m-1) [m\xi^2 (\xi T - m f^2 J) - 5/4\, (n-1)\, \xi T^2] + 2m^2 (\xi^2 - \lambda)(m f^2 J - \xi T)\} = 0 \end{aligned} \tag{2.17}$$

n is the square of the Mach number for the fast magnetosonic mode. t has a more subtle interpretation and is discussed below. In equation (2.18a), v_θ is the fluid velocity in the θ-direction in spherical geometry. Equations (2.12) and (2.17) fully specify the flow and a solution can be obtained by integrating equation (2.17) numerically using the initial conditions $\xi(0) = 1$ and $\xi'(0) = \xi_0'$, with f given implicitly by equation (2.12).

2.4 CRITICAL POINTS

Critical points of the differential equation usually arise in stationary flows where the fluid velocity equals the speed of a backward-propagating disturbance. As such, they are a relic of the initial conditions, since the waves are propagating along the characteristics of the time-dependent equations. There are two appropriate waves in this problem, the non-compressive Alfvén mode and the compressive fast magnetosonic mode. The mathematical behaviour of the solutions is most transparent if we replace equation (2.17) with the equation for the Alfvén Mach number,

$$m' = \frac{mS^2\{2m^2\chi(\xi^2-\lambda)J-(m-1)(5/4T+\xi^2-S)\xi(\chi+\xi\xi') \\ -(m-1)^2[\chi(\xi^2+T)-f^2(\chi+\xi\xi')]J\}}{\xi T(m-1)(t-1)}. \tag{2.20}$$

This equation has two important possible singularities. Firstly, when $m=1$, the denominator becomes zero and so, for a physical solution to pass through $m=1$, the numerator must also be zero. This implies that $\xi=\lambda^{1/2}$, the usual condition for an Alfvén critical point (*cf.* Weber & Davis 1967). However, in this problem the interpretation is somewhat more subtle than in spherically symmetric problems. Our flow has, by mathematical assumption, been constrained to be both axisymmetric and self-similar. This is also true of the corresponding

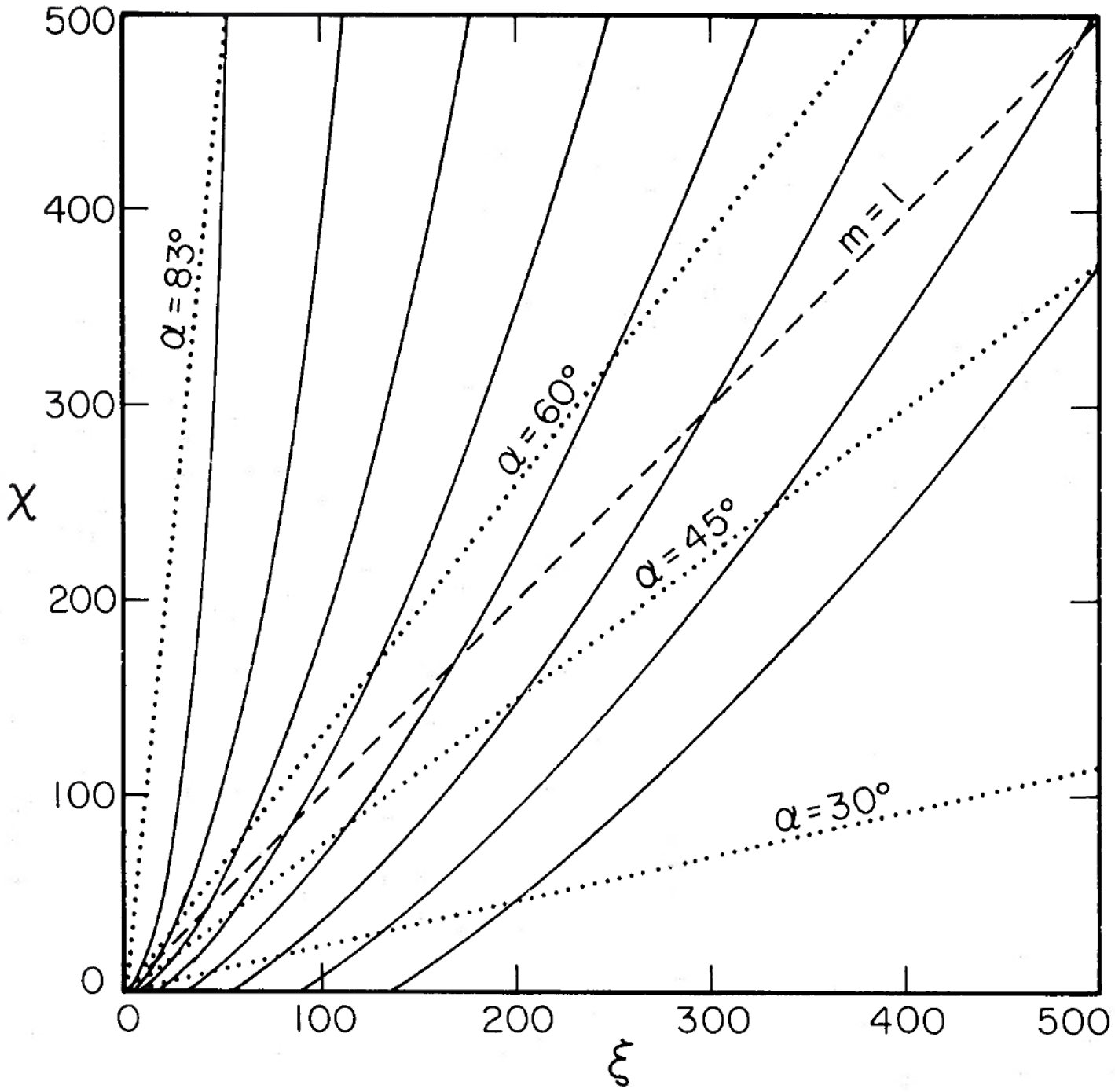
500
400
300
200
100
0
χ
0
100
200
300
400
500
ξ
α=83°
α=60°
α=45°
α=30°
m=1

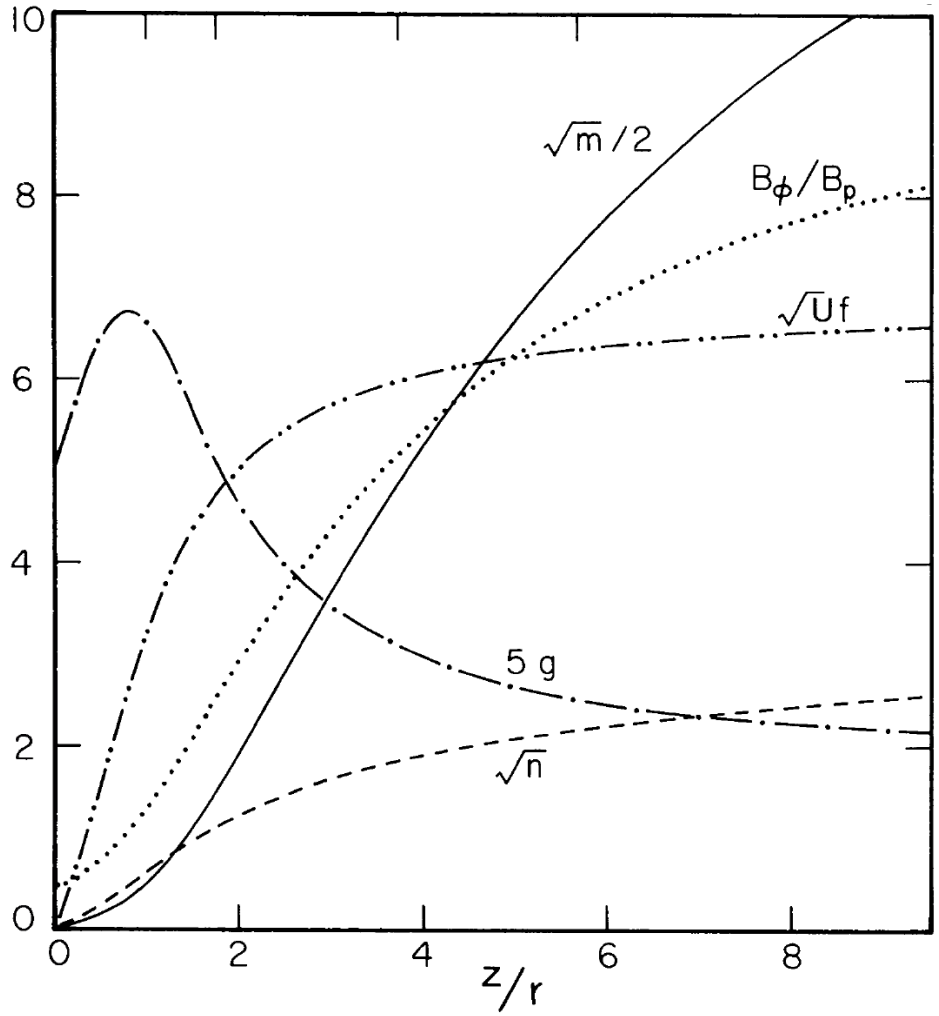

Figure 4. The Alfvén Mach number $m^{1/2}$, the fast magnetosonic Mach number $n^{1/2}$, the poloidal velocity $U^{1/2}f$, the toroidal velocity g, and the ratio of the toroidal field strength to the poloidal field strength along a single streamline.

$$\nabla \cdot (\rho \boldsymbol{v}) = 0 \,,$$

$$\nabla \times \boldsymbol{B} = \frac{4\pi}{c} \boldsymbol{J} \,,$$

$$\boldsymbol{E} + \frac{1}{c} \boldsymbol{v} \times B = 0 \,,$$

$$\nabla \times \boldsymbol{E} = 0 \,,$$

$$\rho(\boldsymbol{v} \cdot \nabla)\boldsymbol{v} = -\nabla p + \rho \boldsymbol{g} + \frac{1}{c} \boldsymbol{J} \times \boldsymbol{B} \,,$$

$$\nabla \cdot \boldsymbol{B} = 0 \,,$$

the *generalized, nonrelativistic Grad-Shafranov equation* for $\Psi(r, z)$ (LMMS):

$$\left(1 - \frac{F^2}{4\pi\rho}\right)\Delta^*\Psi - F\nabla\left(\frac{F}{4\pi\rho}\right) \cdot \nabla\Psi = -4\pi\rho r^2(J' + r v_\phi \Omega') - (H + r v_\phi F)(H' + r v_\phi F') + 4\pi r^2 p(S'/k_B)$$

$$\Delta^* \equiv r \frac{\partial}{\partial r} \frac{1}{r} \frac{\partial}{\partial r} + \frac{\partial^2}{\partial z^2} \,,$$

"Magnetically driven jets and winds: Exact solutions",
Contopoulos & Lovelace 1994

$$\Psi(r, z) = (r_\Psi)^x \Psi_0 \qquad \boldsymbol{B}(r, z) = (r_\Psi)^{x-2} \boldsymbol{B}(Z)$$

$$\boldsymbol{v}(r, z) = (r_\Psi)^{-1/2} \boldsymbol{V}(Z) \boldsymbol{v}_0$$

$$R'' = \frac{\mathscr{F}}{\mathscr{G}}(R, R', Z),$$

where

$$\begin{aligned}
\mathscr{F}(R, R', Z) = &- [1 - F_0 V_z R(R - ZR')] \left[- \frac{1}{R(R - ZR')} + (x - 1) \frac{1 + (R')^2}{(R - ZR')^2} \right] \\
&+ F_0 \left\{ - \frac{Z + RR'}{(R - ZR')^2} [\mathscr{A} R(R - ZR') + V_z R'(R - ZR')] + V_z R(R - ZR') \left(\frac{3}{2} - x \right) \frac{1 + (R')^2}{(R - ZR')^2} \right\} \\
&+ F_0 \frac{R}{V_z(R - ZR')} \left(J_0 + R V_\phi \frac{3}{2} \Omega_0 \right) - (H_0 + R V_\phi F_0) \left[(x - 1) H_0 + R V_\phi \left(x - \frac{3}{2} \right) F_0 \right] \\
&+ 4\pi R^2 C_s^2 \left[\frac{F_0}{4\pi} \frac{1}{V_z R(R - ZR')} \right] \frac{(2x - 4) - \Gamma(2x - 3)}{\Gamma(\Gamma - 1)},
\end{aligned}$$

and

$$\mathscr{G}(R, R', Z) = [1 - F_0 V_z R(R - ZR')] \left[- \frac{R^2 + Z^2}{(R - ZR')^3} \right] + F_0 \frac{Z + RR'}{(R - ZR')^2} [\mathscr{B} R(R - ZR') - V_z RZ].$$

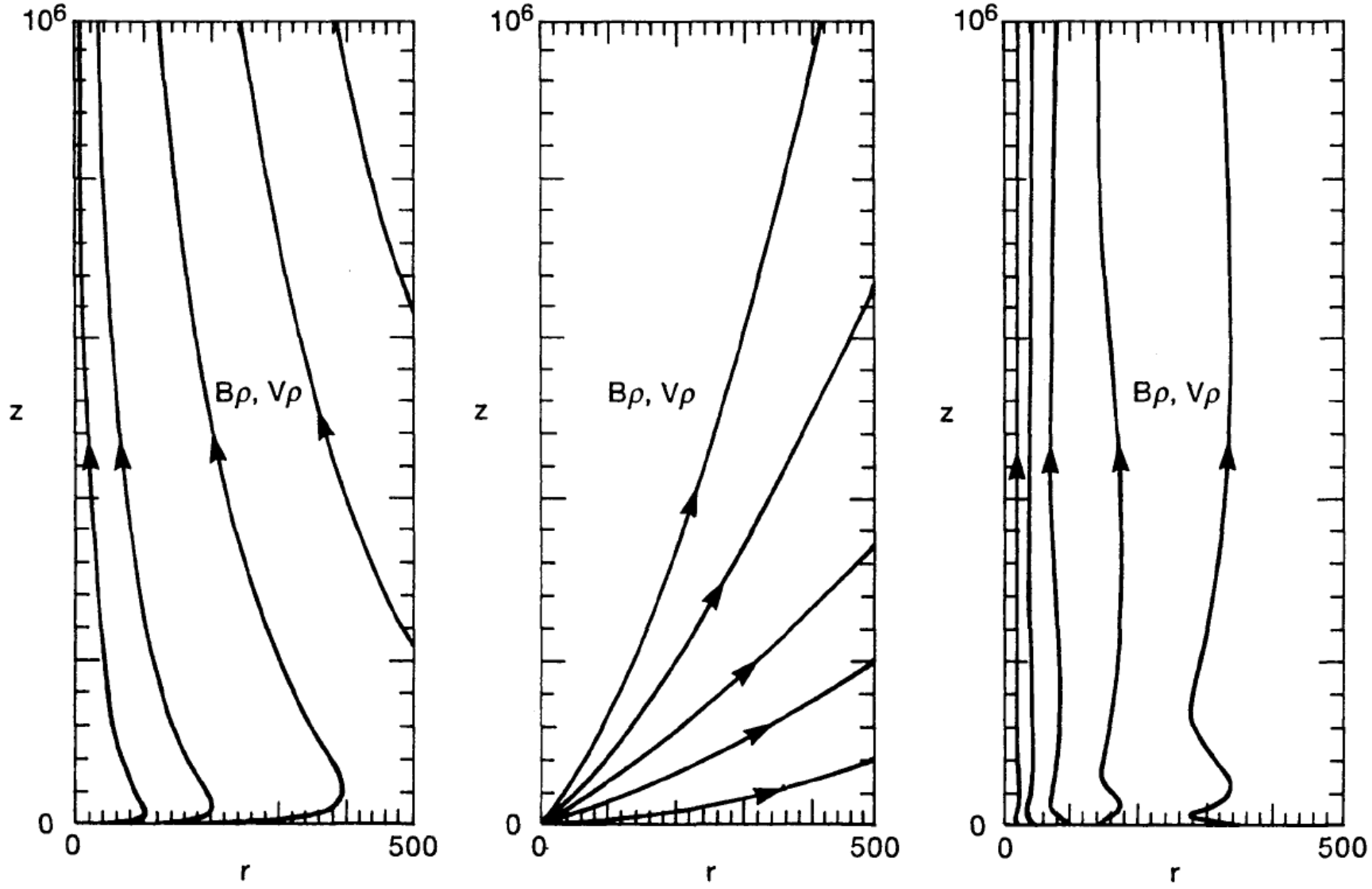

"Magnetically driven jets and winds: Exact solutions",
Contopoulos & Lovelace 1994

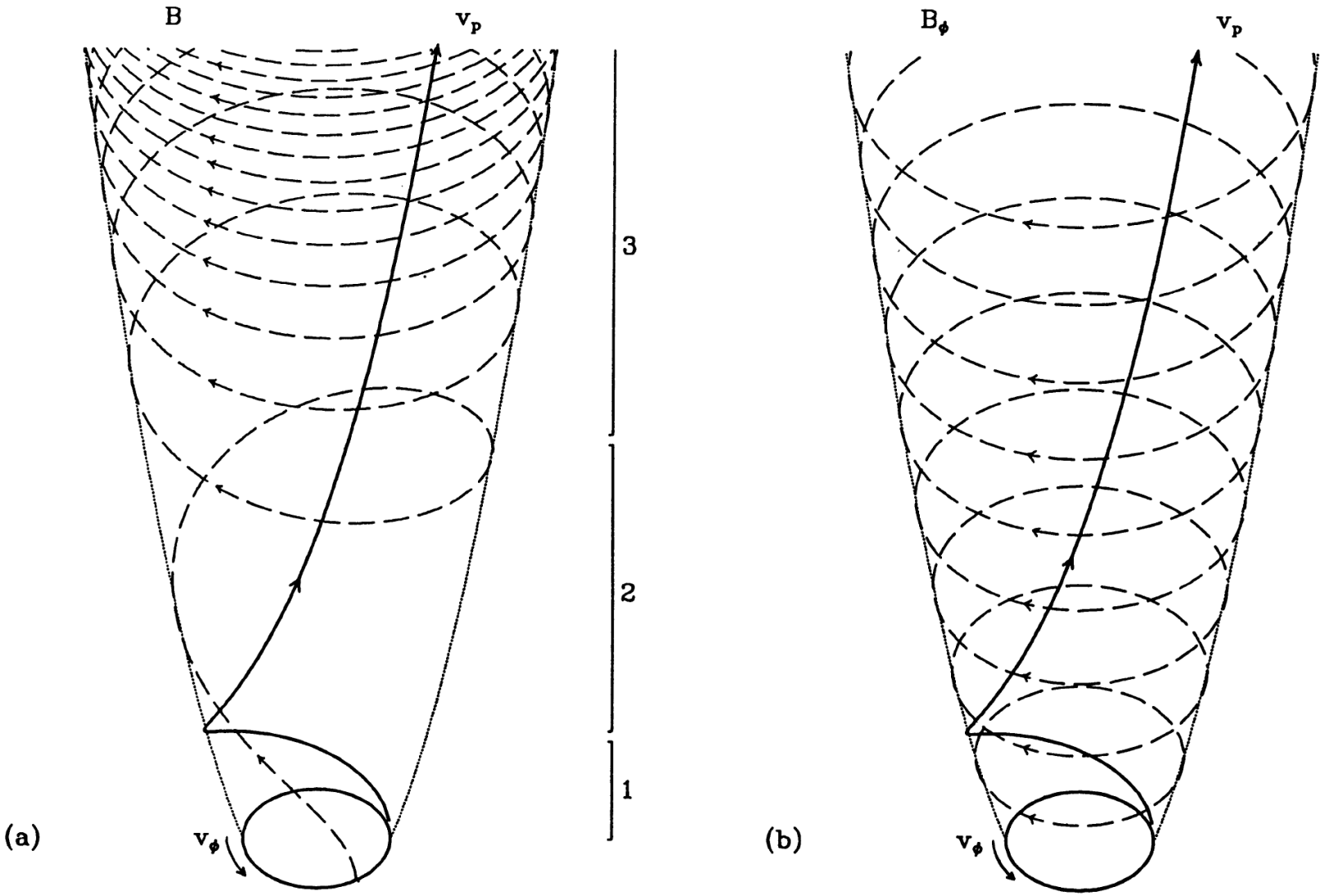

"A simple type of magnetically driven jets: an astrophysical plasma gun", Contopoulos 1995

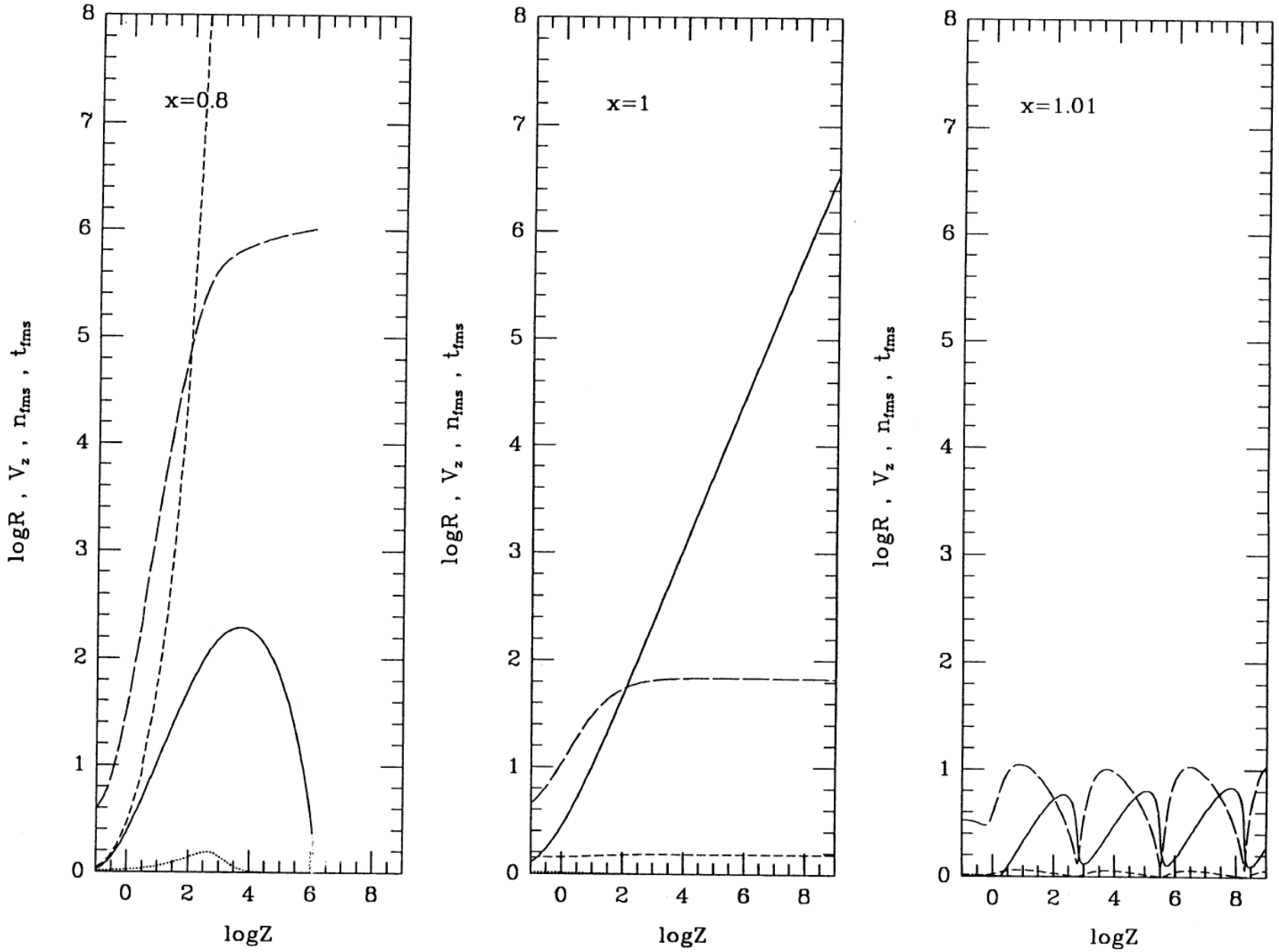

"A simple type of magnetically driven jets: an astrophysical plasma gun", Contopoulos 1995

“Magnetohydrodynamic disk-wind connection”, Li Zhi-Yun 1995-96

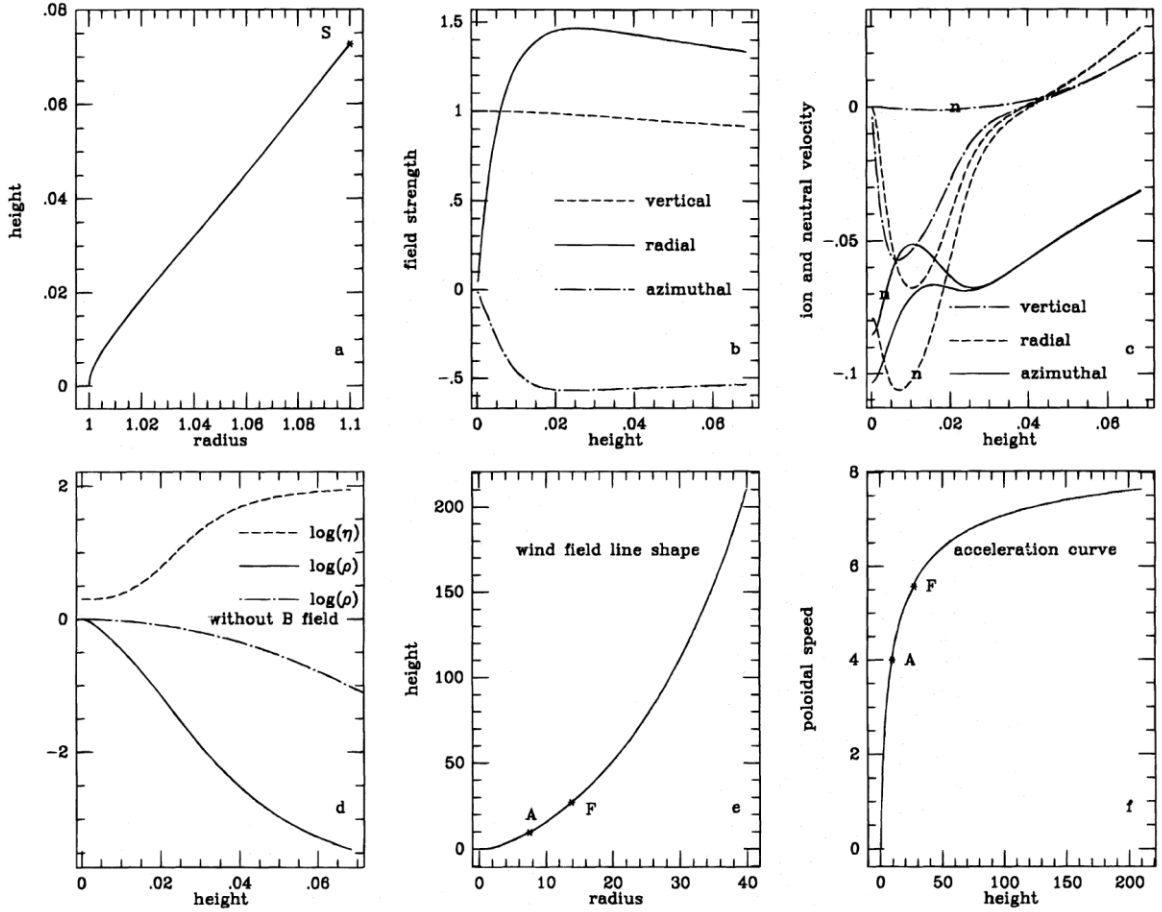

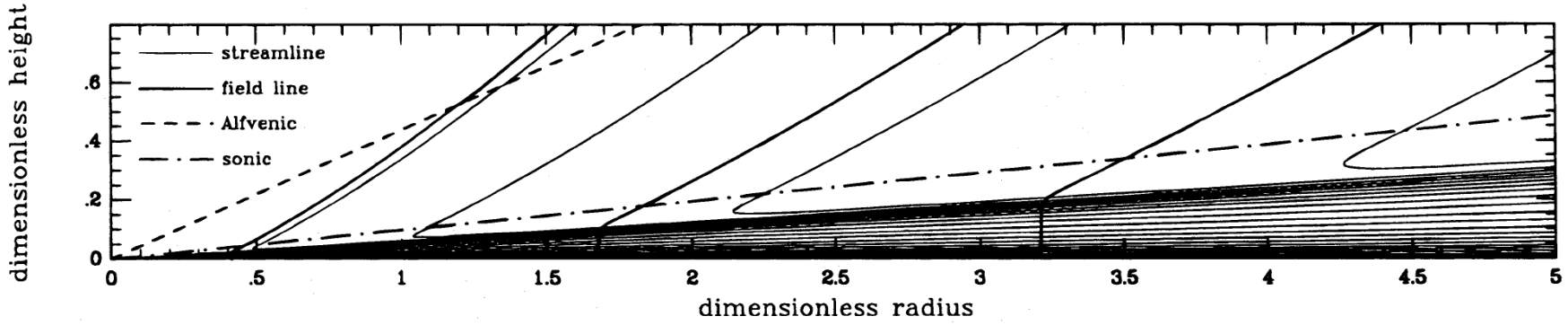

FIG. 3.—Plotted are the poloidal magnetic field lines (*heavy solid lines*) and the poloidal streamlines (*light solid lines*) for the critical disk-wind solution displayed in Fig. 2. This figure shows clearly how a small fraction of the disk material near the surface of the disk is turned around and accelerated through the sonic (*dot-dashed line*) and the Alfvén point (*dashed line*) to form a wind.

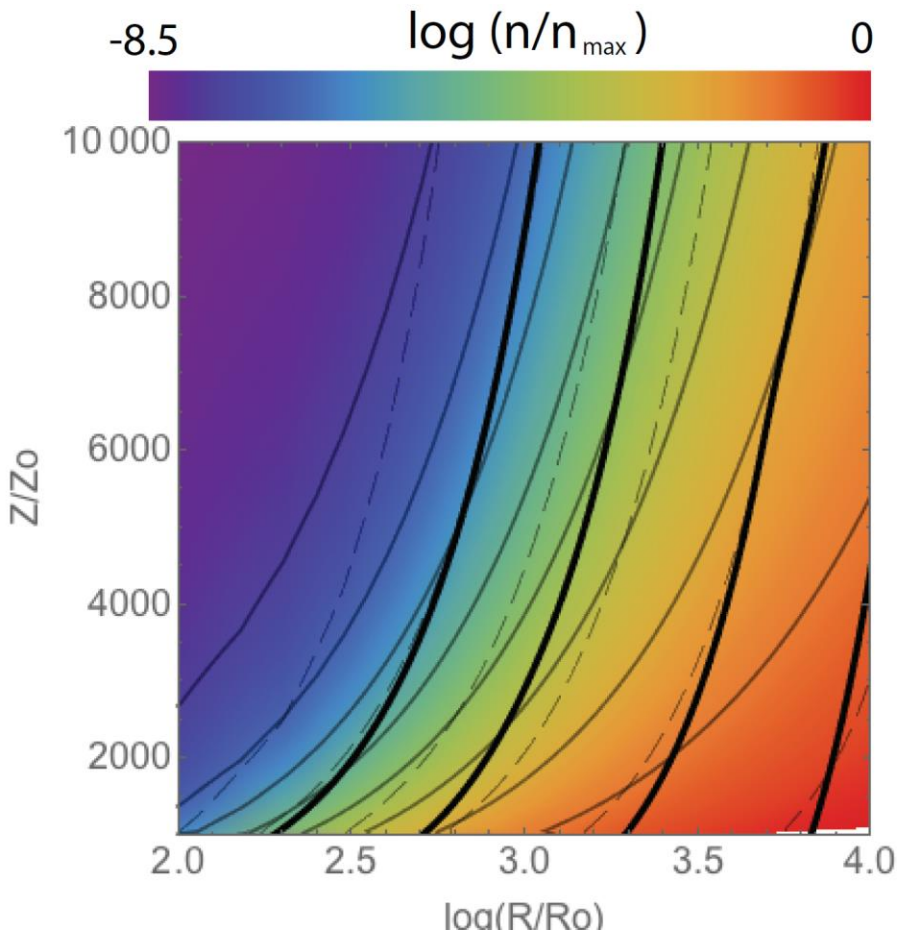

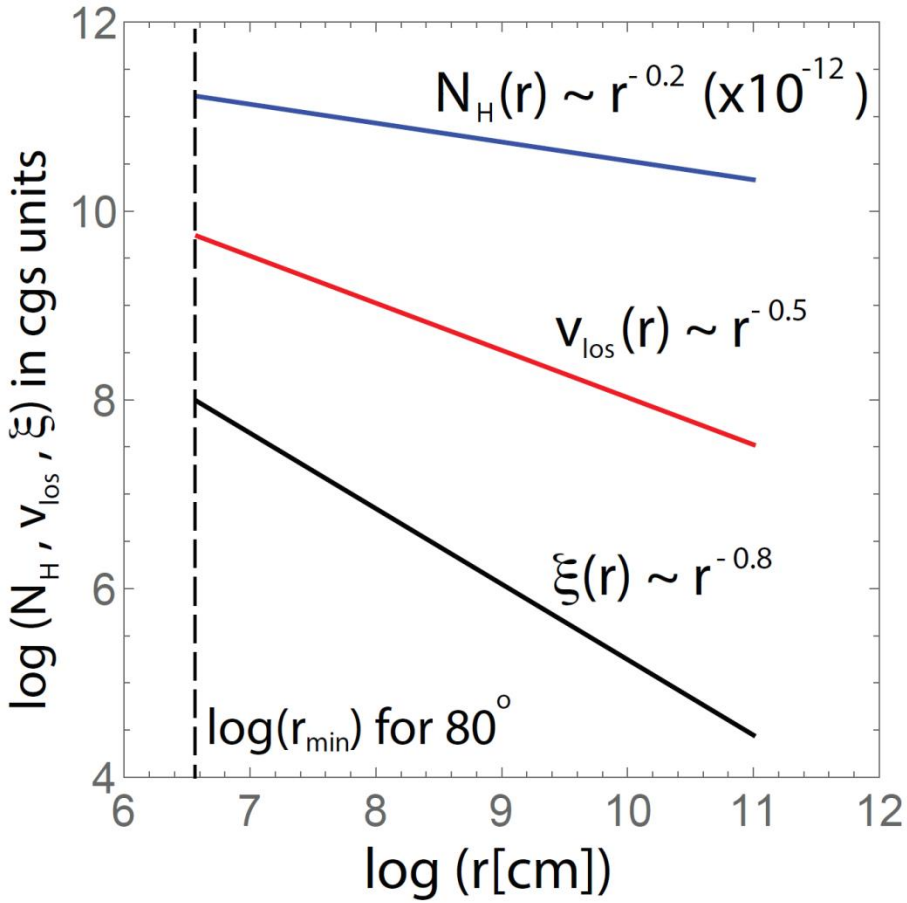

"The universal magnetic structure of black hole accretion disk winds", Fukumura et al. 2016

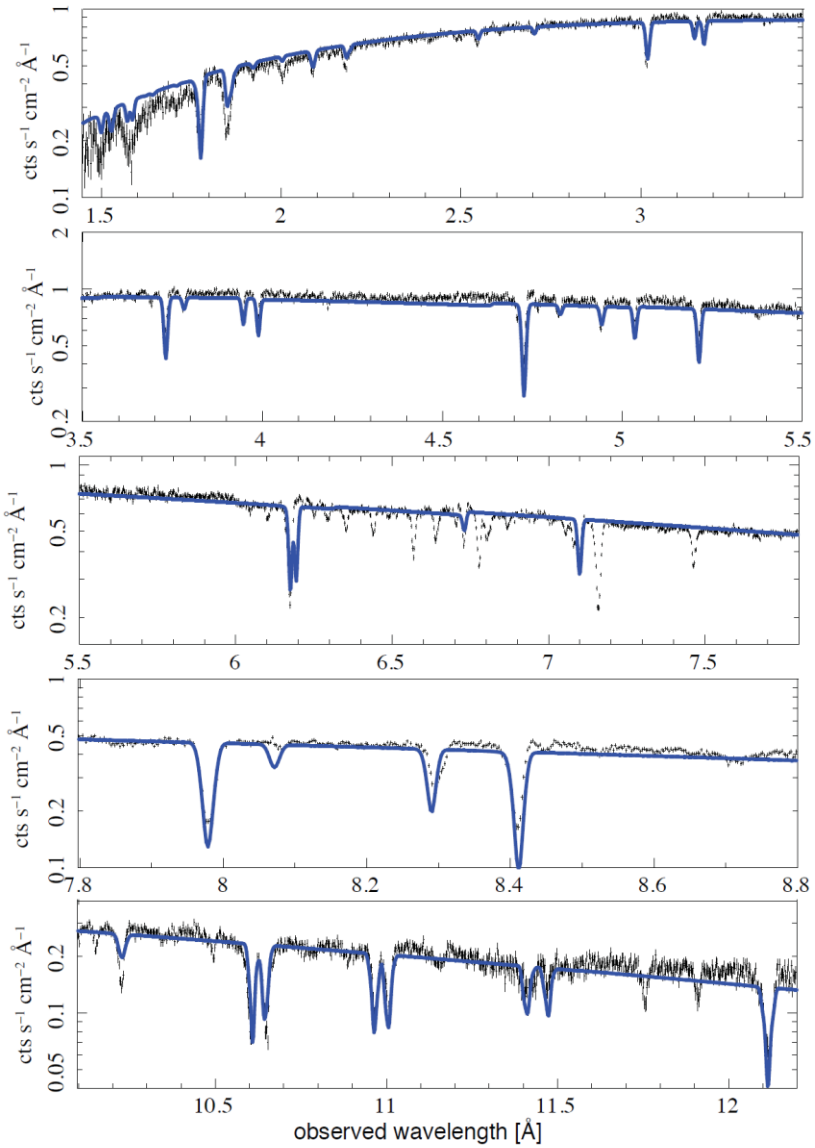

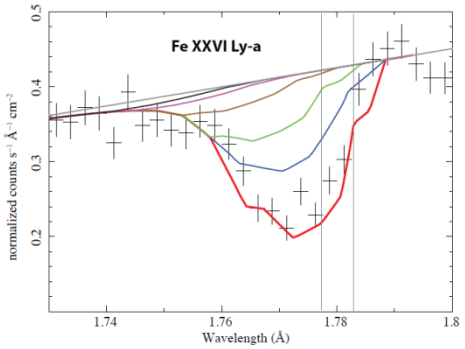

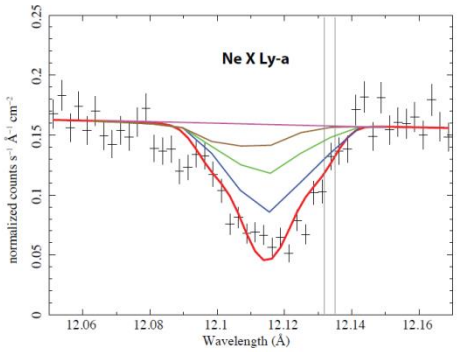

"The universal magnetic structure of black hole accretion disk winds", Fukumura et al. 2016

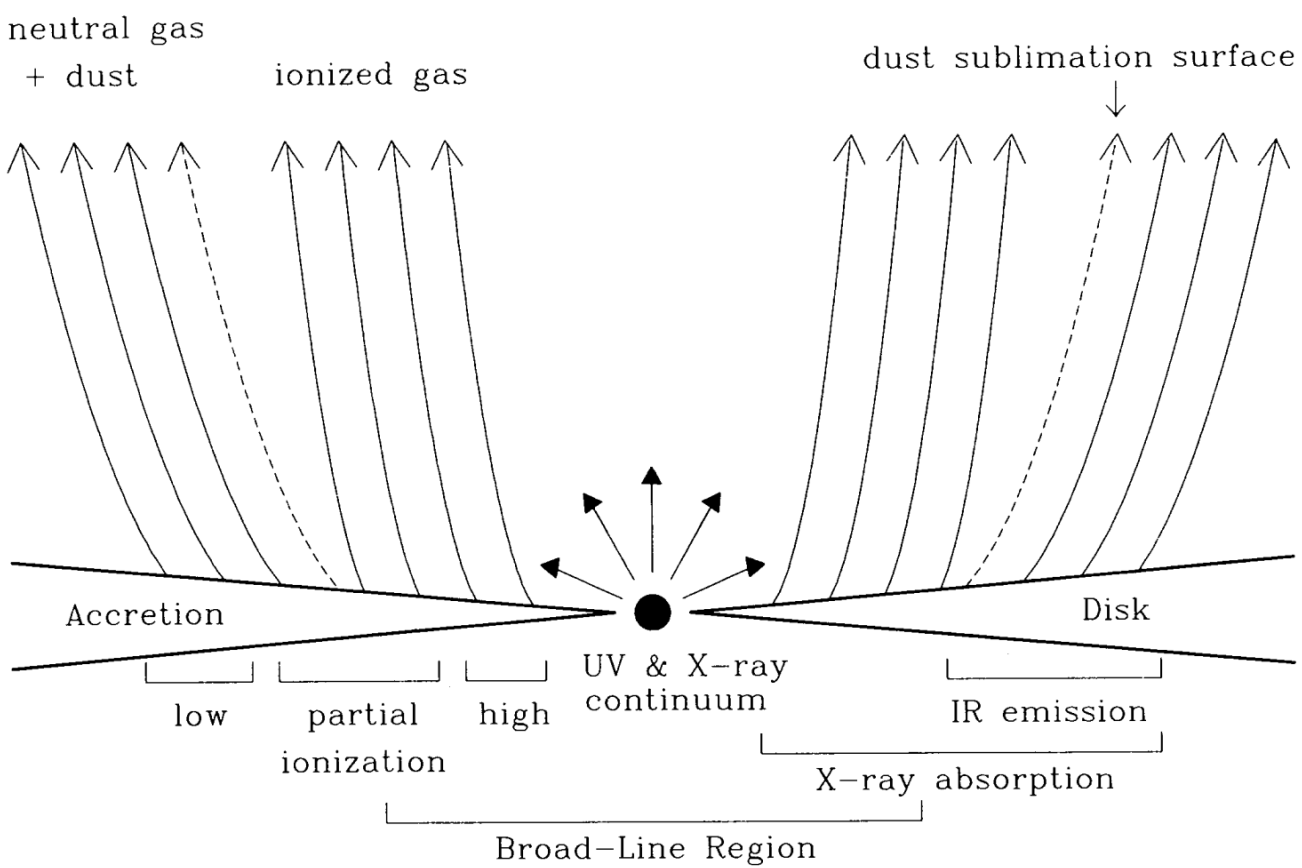

FIG. 13.—Schematic representation of how a disk-driven hydromagnetic wind, which is characterized by a highly stratified density distribution, interacts with the active galactic nucleus (AGN) continuum emission. The innermost regions are heated and ionized by the powerful radiation field, with the temperature and degree of ionization varying both with distance and with the polar angle, whereas the outer regions (beyond the dust sublimination radius) are cooler and contain dust. The radiation pressure force on the dust causes the outer streamlines to have a larger opening angle.

"Disk-driven hydromagnetic winds as a key ingredient of active galactic nuclei unification schemes", Konigl & Kartje 1993

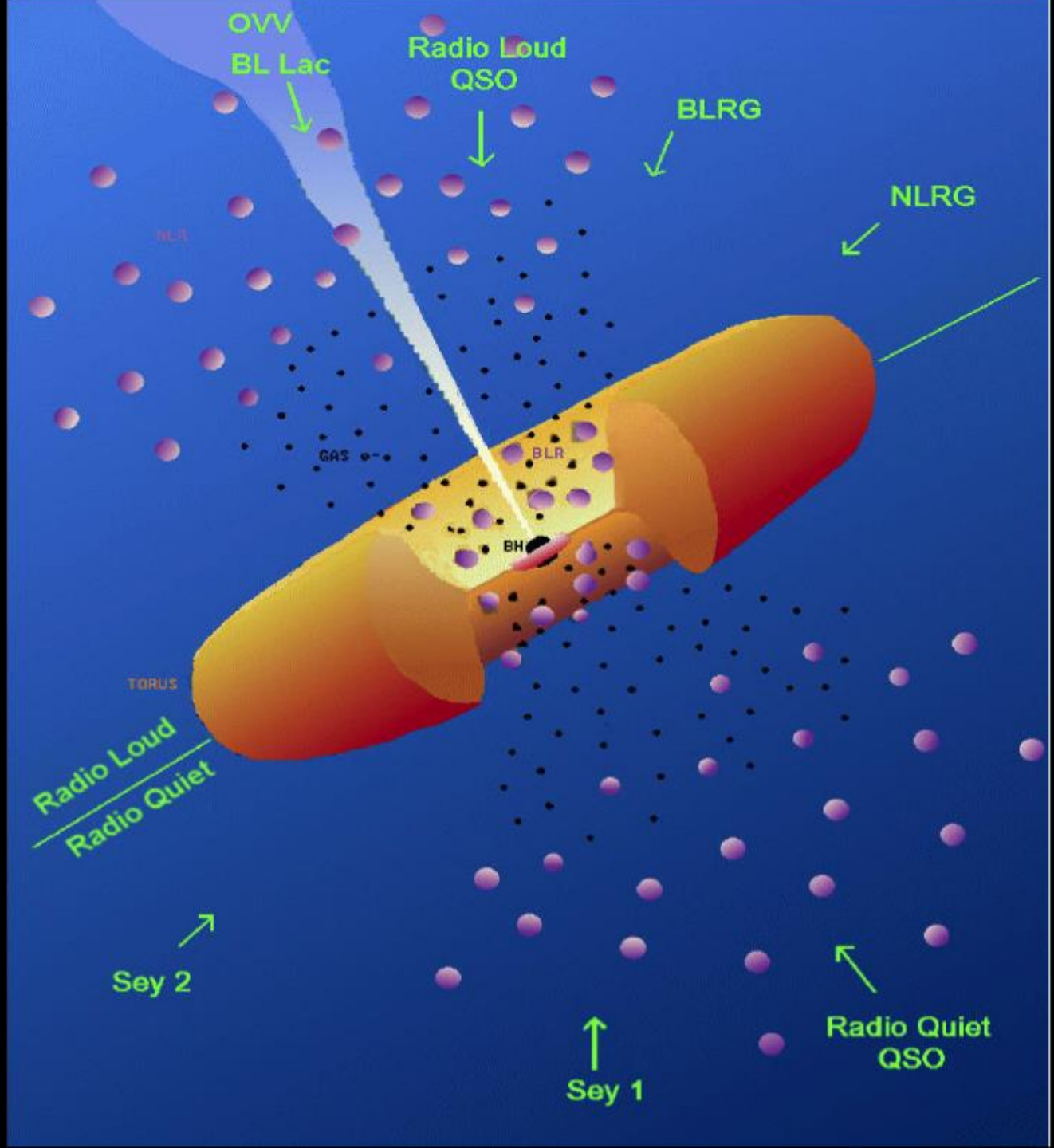
OVV
BL Lac
Radio Loud
QSO
BLRG
NLRG
NLR
GAS
BLR
BH
TORUS
Radio Loud
Radio Quiet
Sey 2
Sey 1
Radio Quiet
QSO

The launching of MHD jets from astrophysical black holes

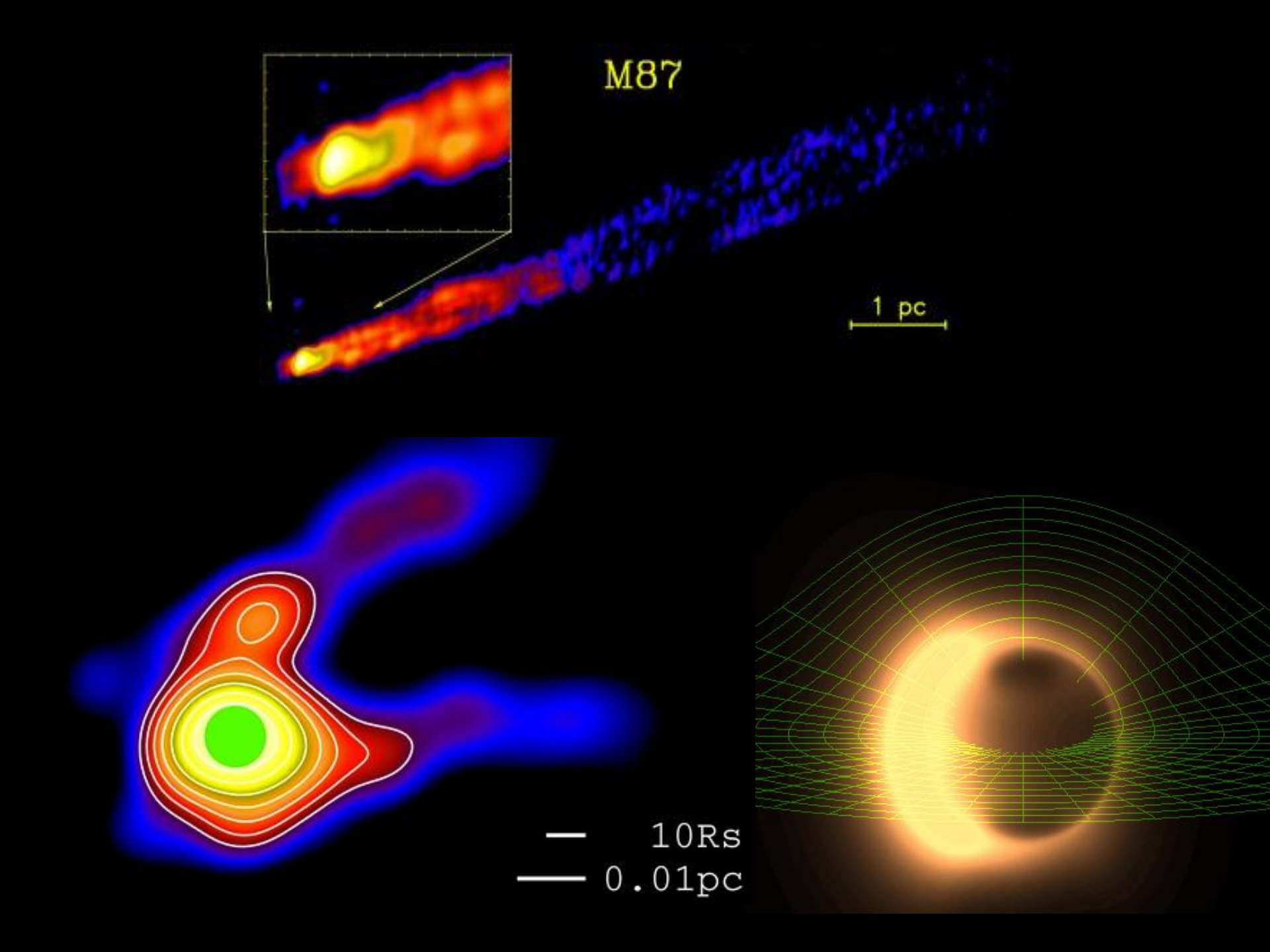
M87
1 pc
10Rs
0.01pc

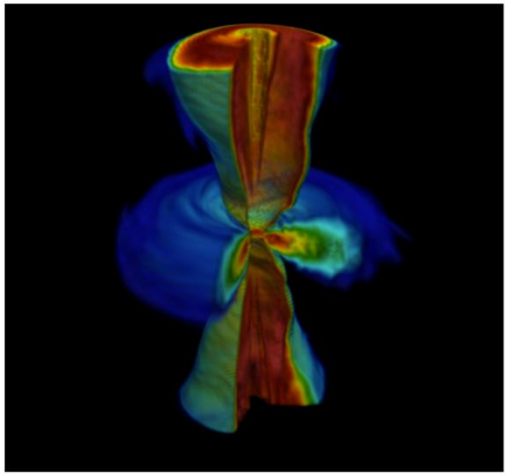

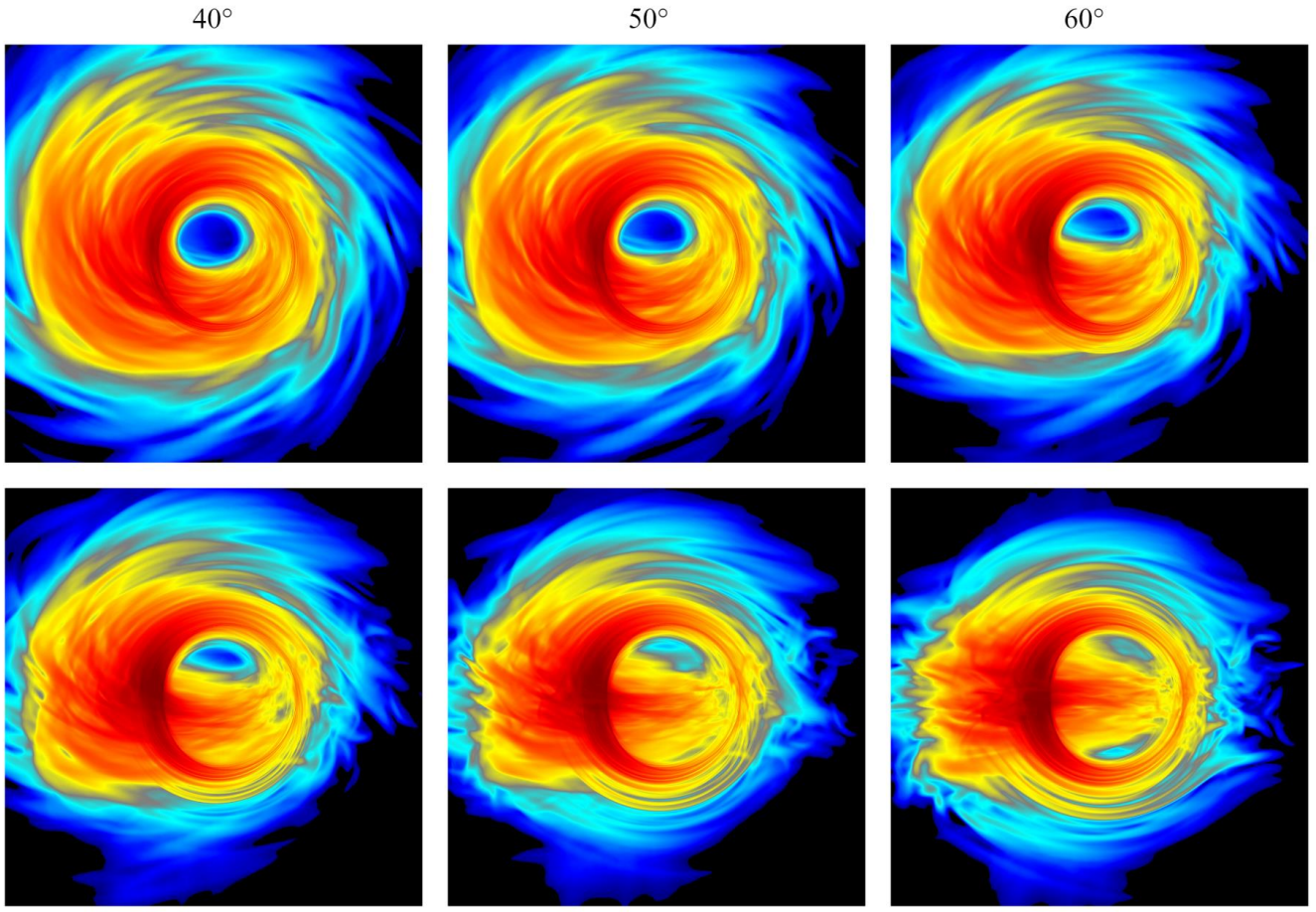

230 GHz (1.3 mm) images (logarithmically stretched) computed by time-dependent relativistic ray-tracing through a 4D GRMHD data hypercube. Inclinations shown are relative to the black hole spin axis (which points along the funnel in the volume rendered image above).

Resolved Spine-sheath Parabolic Streams?

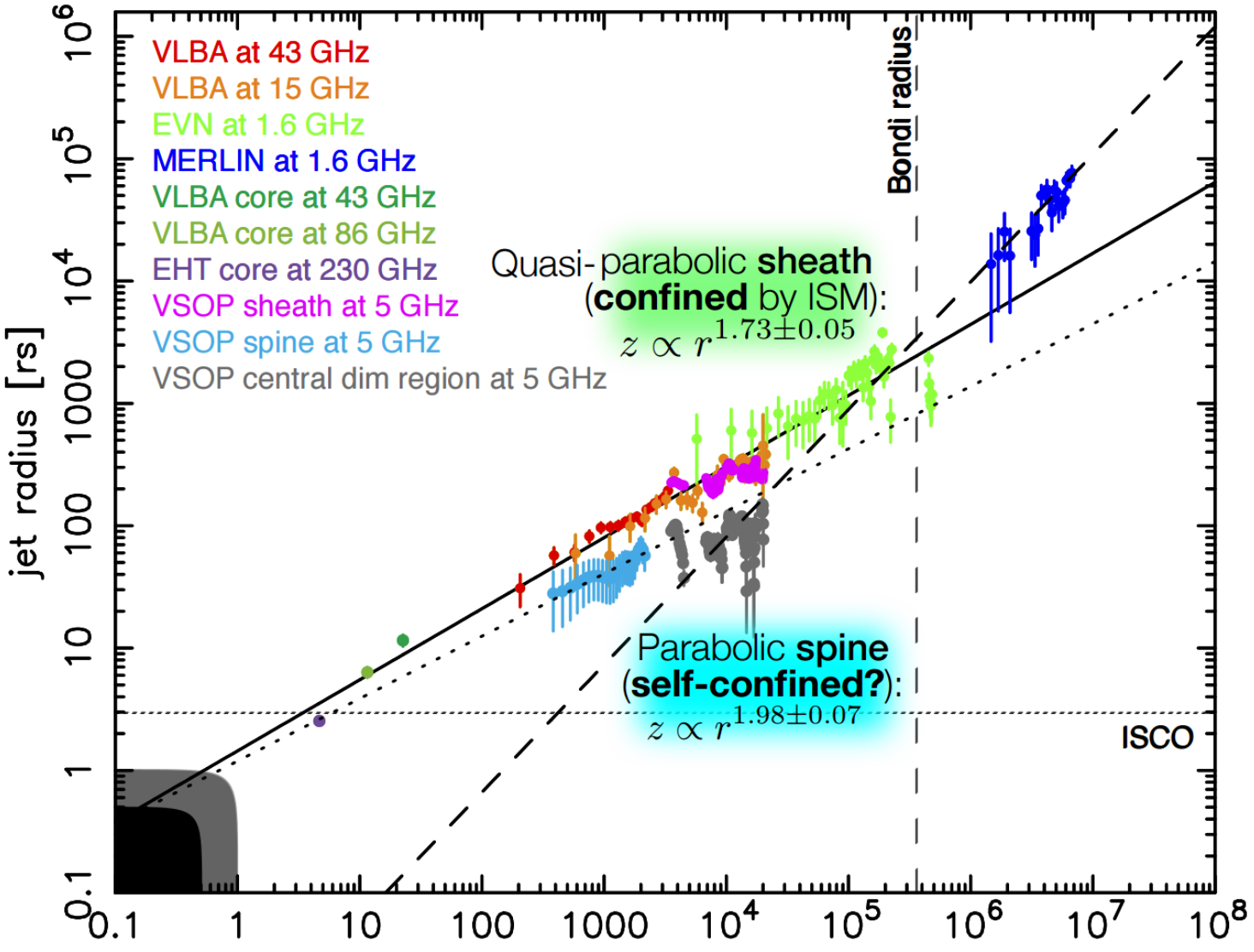

Asada & MN (2012), *ApJL*; MN & Asada (2013), *ApJ*; Asada & MN, in prep.

- “Electromagnetic extraction of energy from Kerr black holes”, Blandford & Znajek 1977
- “Black hole magnetospheres”, Nathanail & Contopoulos 2014
- “Efficient generation of jets from magnetically arrested accretion on a rapidly spinning black hole”, Tchekhovskoy, Narayan, McKinney 2011-

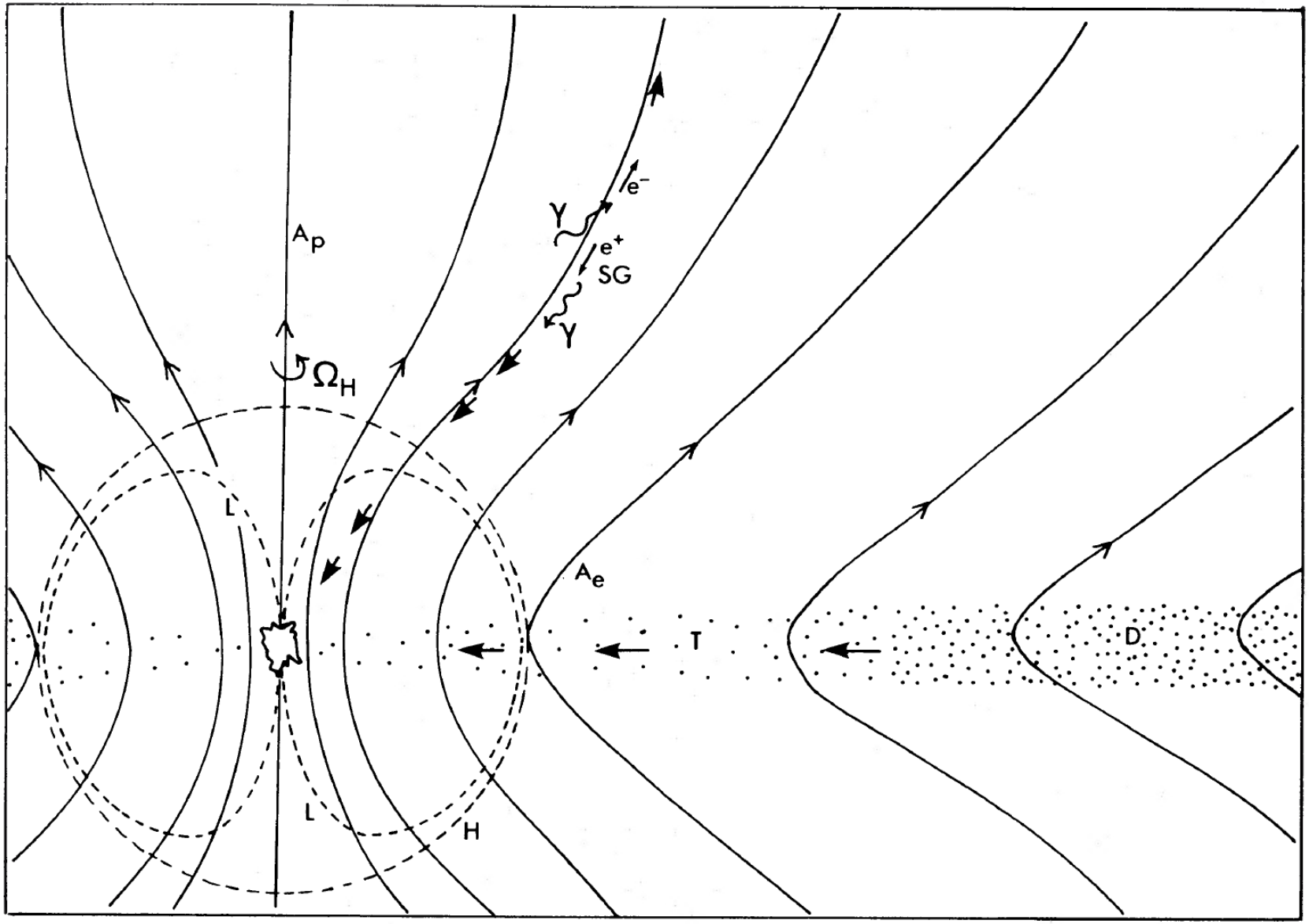

"Electromagnetic extraction of energy from Kerr black holes",
Blandford & Znajek 1977

A physical observer rotating at constant radius close to the horizon will in general see a Poynting flux of energy entering the hole, but he will also see a sufficiently strong flux of angular momentum leaving the hole to ensure that $\mathscr{E}^r \gtrsim 0$. Equations (3.15) and (4.3) show that at the event horizon

$$\mathscr{E}^r = \omega(\Omega_H - \omega)\left(\frac{A_{\phi,\theta}}{r_+^2 + a^2\cos^2\theta}\right)^2 (r_+^2 + a^2)\,\epsilon_0 \tag{4.5}$$

where $\Omega_H \equiv a/(r_+^2 + a^2)$ is the angular velocity of the hole (e.g. Misner *et al.* 1973). Hence $\mathscr{E}^r \gtrsim 0$ implies

$$0 \lesssim \omega \lesssim \Omega_H, \tag{4.6}$$

$$\dot{E} \approx -\frac{1}{6\pi c}\Psi_m^2\Omega^2 \approx 10^{44} \ \text{erg/s}$$

"Electromagnetic extraction of energy from Kerr black holes",
Blandford & Znajek 1977

$$ds^2 = -\alpha^2 dt^2 + \varpi^2 (d\phi - \Omega dt)^2 + \frac{\Sigma}{\Delta} dr^2 + \Sigma d\theta^2, \quad (1)$$

where

$$\alpha = (\Delta\Sigma/A)^{1/2},$$

$$\Omega = 2aMr/A,$$

$$\varpi = (A/\Sigma)^{1/2} \sin\theta,$$

$$\Sigma = r^2 + a^2 \cos^2\theta$$

$$\Delta = r^2 - 2Mr + a^2,$$

$$A = (r^2 + a^2)^2 - a^2 \Delta \sin^2\theta.$$

Here, M is the mass of the black hole and a its angular momentum ($0 \leqslant a \leqslant M$), α is the lapse function, Ω is the angular velocity of ZAMOs, and ϖ is the cylindrical radius ($\varpi = r \sin\theta$ when $a = 0$). Throughout this paper, we use

where $\mathbf{E}\cdot\mathbf{B} = 0$. Under these assumptions, Maxwell's equations become

$$\nabla \times \mathbf{B} = 0$$

$$\nabla \times \mathbf{E} = 4\pi\rho_e$$

$$\nabla \times (\alpha\mathbf{B}) = 4\pi\alpha\mathbf{J}$$

$$\nabla \times (\alpha\mathbf{E}) = 0\,, \quad (3)$$

and the force-free condition yields

$$\rho_e\mathbf{E} + \mathbf{J} \times \mathbf{B} = 0. \quad (4)$$

Furthermore, the electric ($\mathbf{E}$) and the magnetic ($\mathbf{B}$) field can be expressed in terms of three scalar functions $\Psi(r, \theta)$ (the total magnetic flux enclosed in the circular loop $r = \text{const.}$, $\theta = \text{const.}$ divided by 2π), $\omega(\Psi)$ (the angular velocity of the magnetic field lines), and $I(\Psi)$ (the poloidal electric current flowing through that loop), as

$$\mathbf{B}(r, \theta) = \frac{1}{\sqrt{A}\sin\theta} \left\{ \Psi_{,\theta}\mathbf{e}_{\hat{r}} - \sqrt{\Delta}\Psi_{,r}\mathbf{e}_{\hat{\theta}} + \frac{2I\sqrt{\Sigma}}{\alpha}\mathbf{e}_{\hat{\phi}} \right\} \quad (5)$$

"Black hole magnetospheres", Nathanail & Contopoulos 2014

$$\left\{\Psi_{,rr}+\frac{1}{\Delta}\Psi_{,\theta\theta}+\Psi_{,r}\left(\frac{A_{,r}}{A}-\frac{\Sigma_{,r}}{\Sigma}\right)-\frac{\Psi_{,\theta}}{\Delta}\frac{\cos\theta}{\sin\theta}\right\}$$
$$\times\left[1-\frac{2Mr}{\Sigma}+\frac{4Ma\omega r\sin^2\theta}{\Sigma}-\frac{\omega^2 A\sin^2\theta}{\Sigma}\right]$$
$$+\left(\frac{2Mr}{\Sigma}-\frac{4Ma\omega r\sin^2\theta}{\Sigma}\right)\left(\frac{A_{,r}}{A}-\frac{1}{r}\right)\Psi_{,r}$$
$$+\left(\frac{\Sigma_{,r}}{\Sigma}-\frac{A_{,r}}{A}\right)\Psi_{,r}$$
$$-\left(2\frac{\cos\theta}{\sin\theta}+\frac{A_{,\theta}}{A}-\frac{\Sigma_{,\theta}}{\Sigma}\right)\omega A(\omega-2\Omega)\frac{\Psi_{,\theta}\sin^2\theta}{\Delta\Sigma}$$
$$-2\omega\Omega\varpi^2\frac{\Psi_{,\theta}}{\Delta}\frac{A_{,\theta}}{A}-2Mr\Sigma_{,\theta}\frac{\Psi_{,\theta}}{\Delta\Sigma^2}$$
$$-\frac{\omega' A\sin^2\theta}{\Sigma}(\omega-\Omega)\left(\Psi_{,r}^2+\frac{1}{\Delta}\Psi_{,\theta}^2\right)$$
$$=-\frac{4\Sigma}{\Delta}II' \qquad (7)$$

the general relativistic force-free Grad–Shafranov equation.

$$1-\frac{2Mr}{\Sigma}+\frac{4Ma\omega r\sin^2\theta}{\Sigma}-\frac{\omega^2 A\sin^2\theta}{\Sigma}=0, \qquad (8)$$

yields the singular surfaces of the problem, the so-called LSs where

$$\alpha^{-1}(\omega-\Omega)\varpi=\pm 1 \qquad (9)$$

“Black hole magnetospheres”, Nathanail & Contopoulos 2014

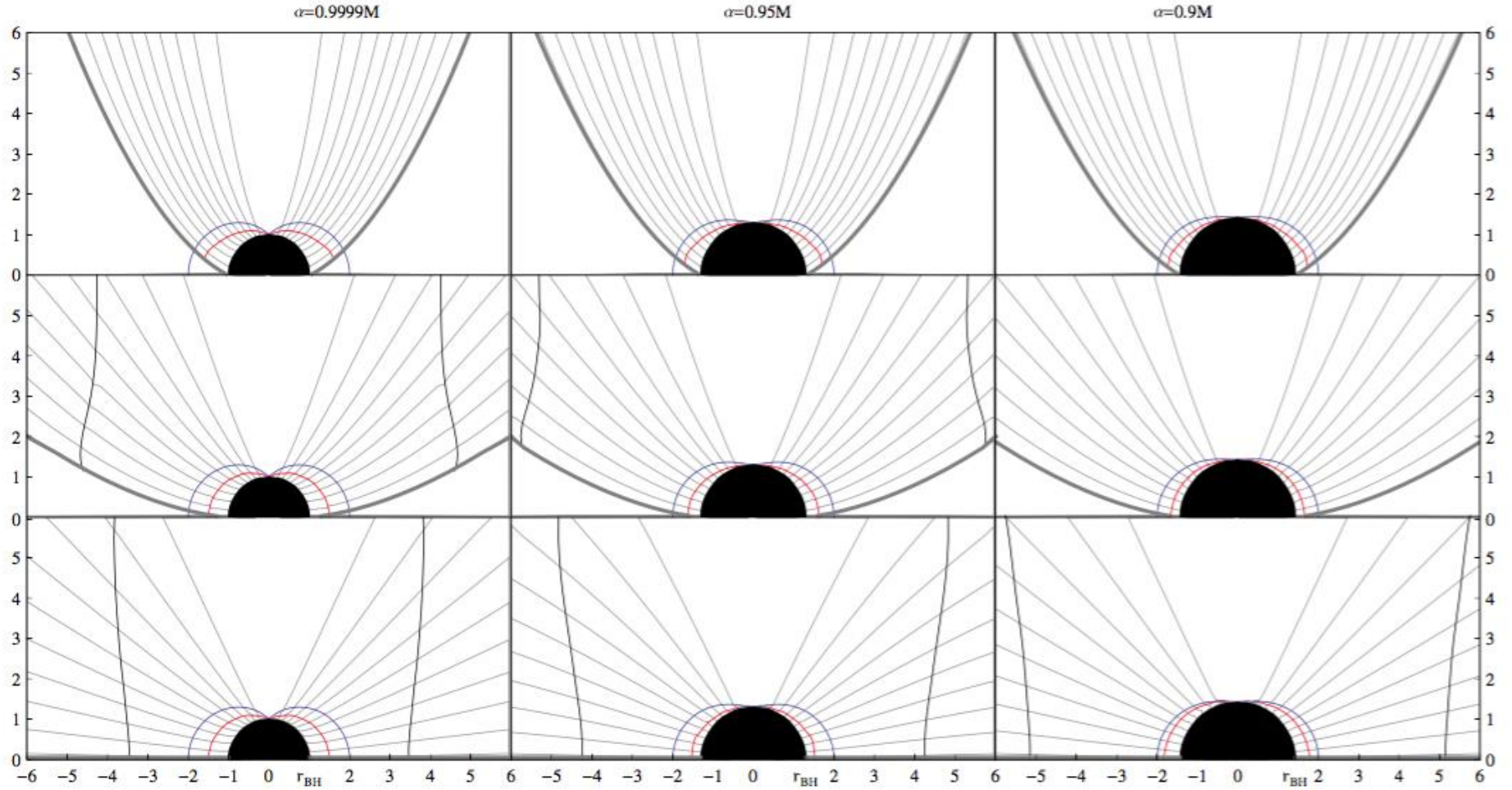

Figure 1. Monopole and paraboloidal solutions. $\nu = 1$. Top to bottom: $r_0 = 1, 10, \infty$. Left to right: $a = 0.9999M, 0.95M, 0.9M$. Black semi-circle: the horizon. Red/blue/black lines: the ILS, the static limit, and the OLS, respectively. Where not seen, the OLS lies outside the region shown. Thick gray line: collimating boundary/equatorial disk.

"Black hole magnetospheres", Nathanail & Contopoulos 2014

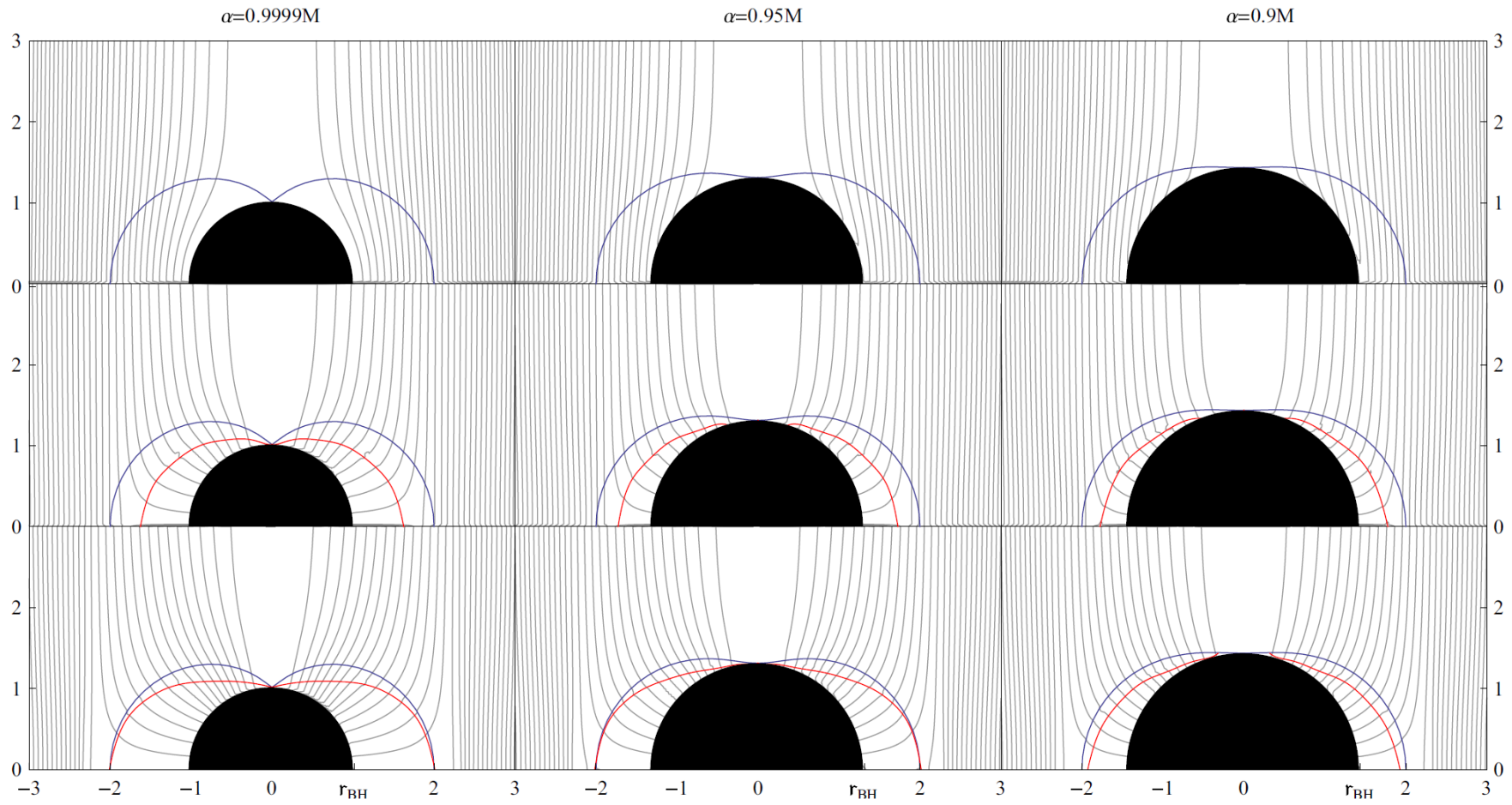

“Black hole magnetospheres”, Nathanail & Contopoulos 2014

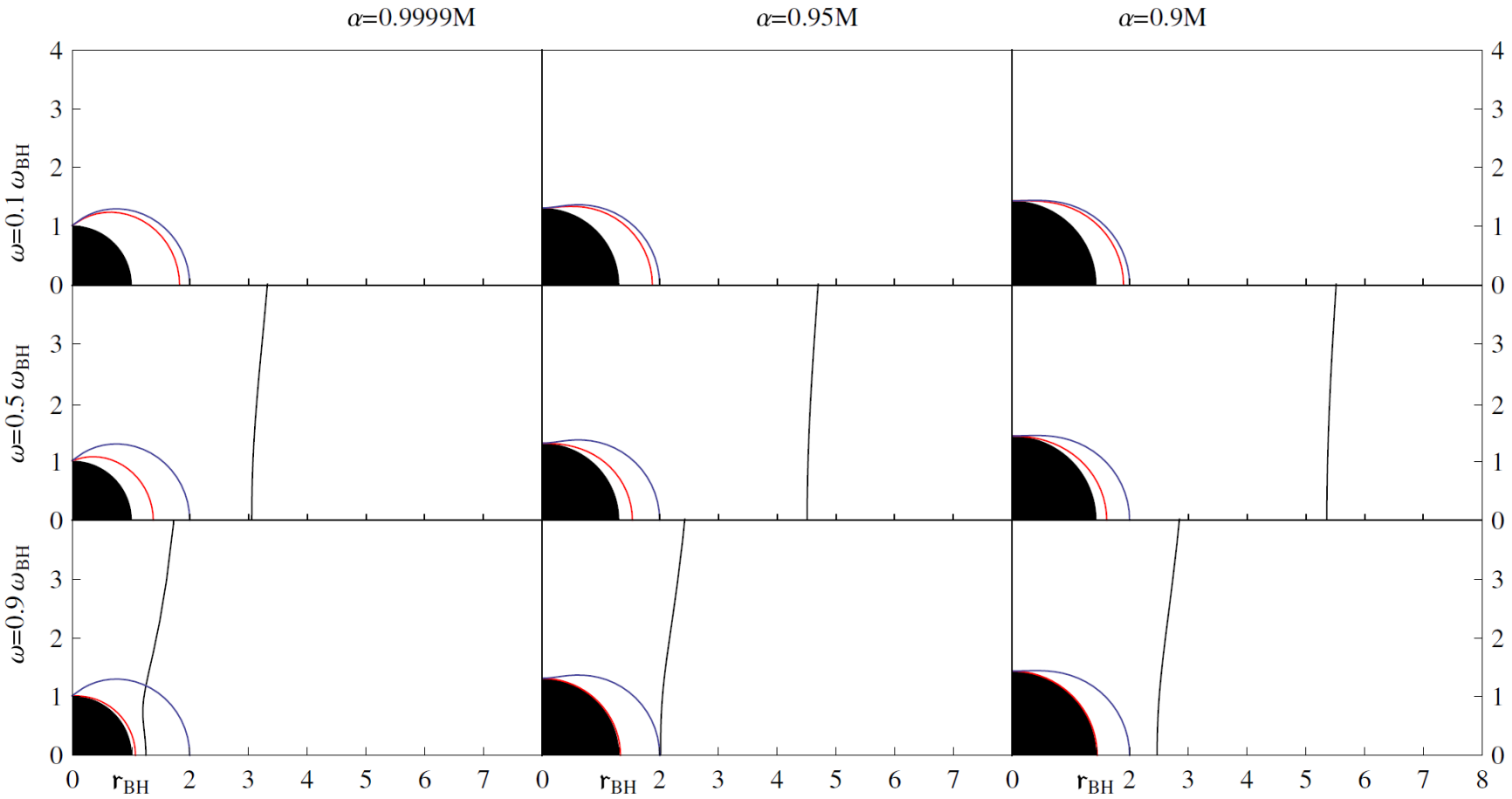

Figure 4. Light surfaces for various black hole spin parameters a and magnetic field angular velocities ω. Line colors as in Figure 1.

"Black hole magnetospheres", Nathanail & Contopoulos 2014

- Wind separation zone (density floors!…)
- Null surface of rotating black hole ($\omega_{ZAMO}=\Omega_{MF}$)
- Black hole gaps (in analogy to pulsars)
- Black hole electron-positron jets!
- Magnetospheric current sheet (in analogy to pulsars)

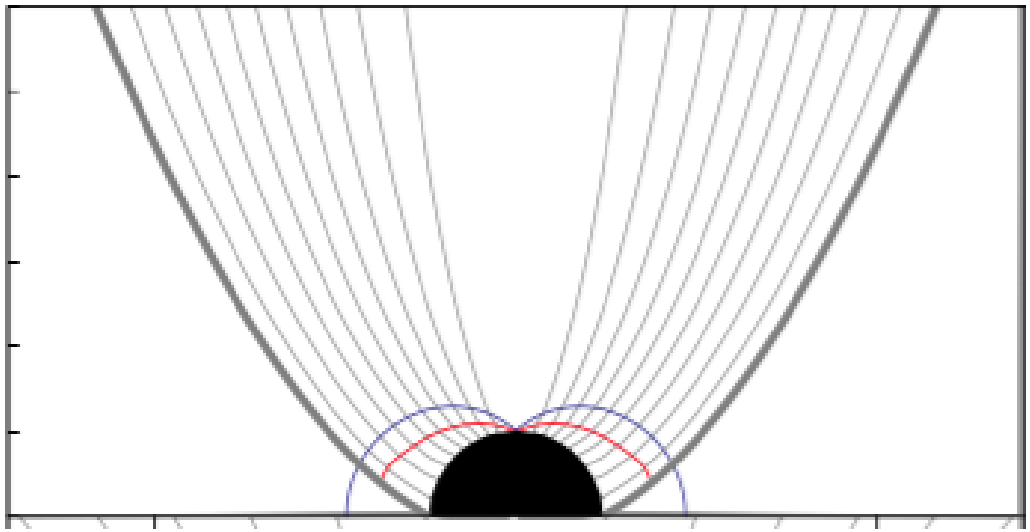

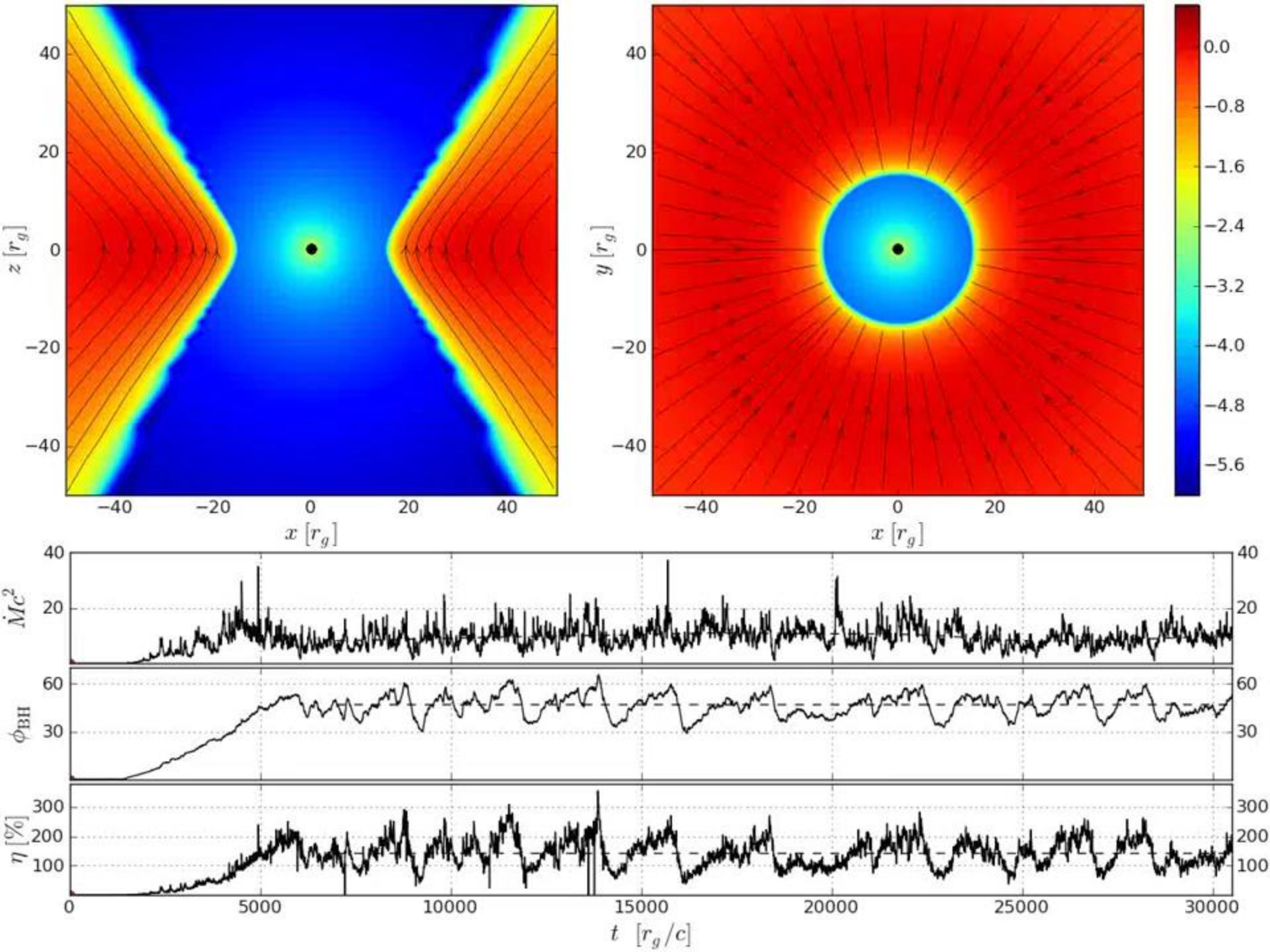
40
20
0
−20
−40
$z\ [r_g]$
−40
−20
0
20
40
$x\ [r_g]$
$y\ [r_g]$
0.0
−0.8
−1.6
−2.4
−3.2
−4.0
−4.8
−5.6
$\dot{M}c^2$
$\phi_{\rm BH}$
$\eta\ [\%]$
60
30
300
200
100
0
5000
10000
15000
20000
25000
30000
$t\ \ [r_g/c]$

The origin of the magnetic field

- “A cosmic battery”, Contopoulos & Kazanas 1998
- “Dominance of outflowing electric currents on decaparsec to kiloparsec scales in extragalactic jets”, Christodoulou et al. 2016

$$E_{\rm CB} = \frac{F_{\rm rad}\,|_{\phi}}{e} = -\frac{L\sigma_{\rm T}}{4\pi c e r^2}\frac{v_{\phi}}{c}$$

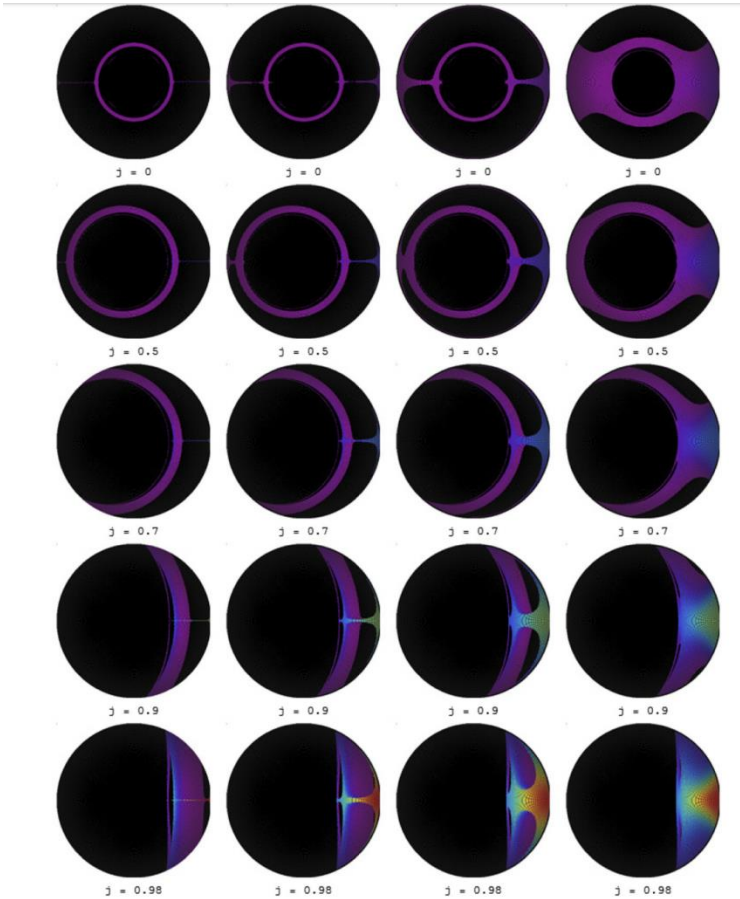

$$\frac{\partial \boldsymbol{B}_{\rm disk}}{\partial t} = -c\nabla \times \left(E_{\rm CB}\hat{\phi} - \frac{\boldsymbol{v}}{c} \times \boldsymbol{B}_{\rm disk} + \eta \nabla \times \boldsymbol{B}_{\rm disk} \right)$$

"Accretion disk radiation dynamics and the cosmic battery",
Koutsantoniou & Contopoulos 2015

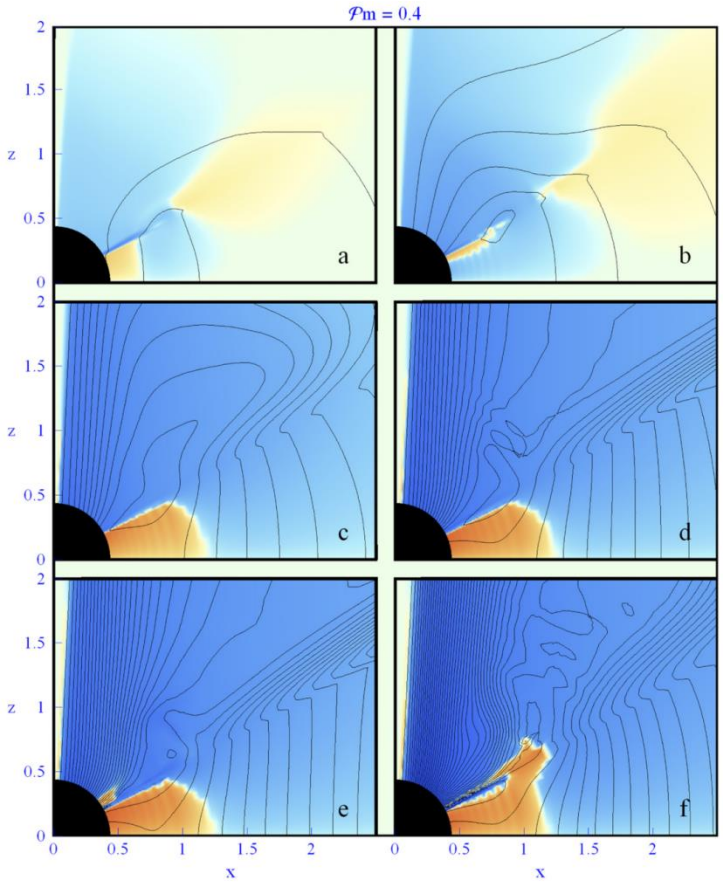
$\mathcal{P}$m = 0.4
a
b
c
d
e
f
z
x
0
0.5
1
1.5
2

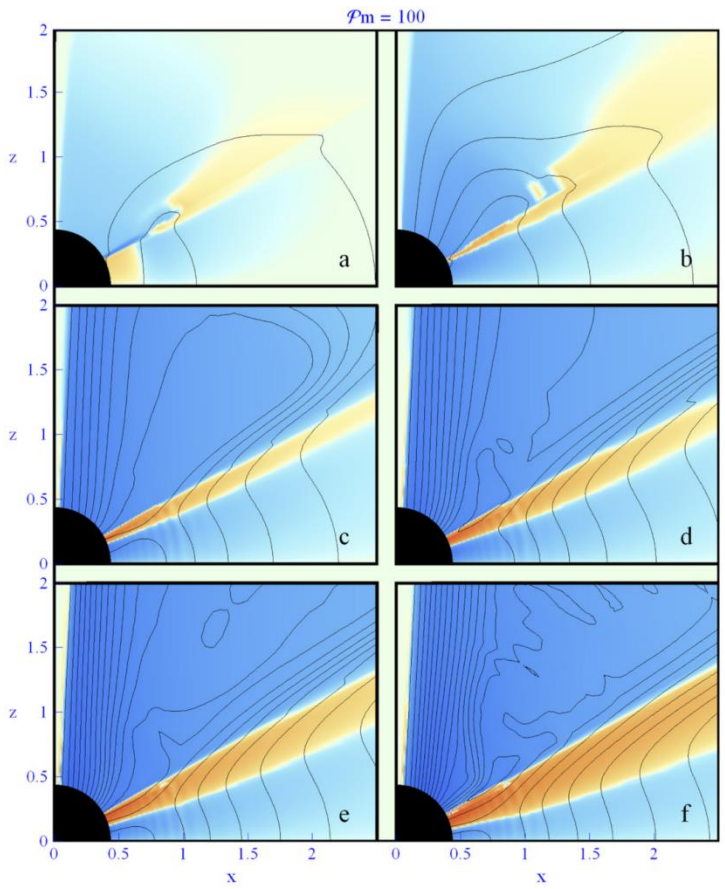
$\mathcal{P}$m = 100
a
b
c
d
e
f
z
x
0
0.5
1
1.5
2

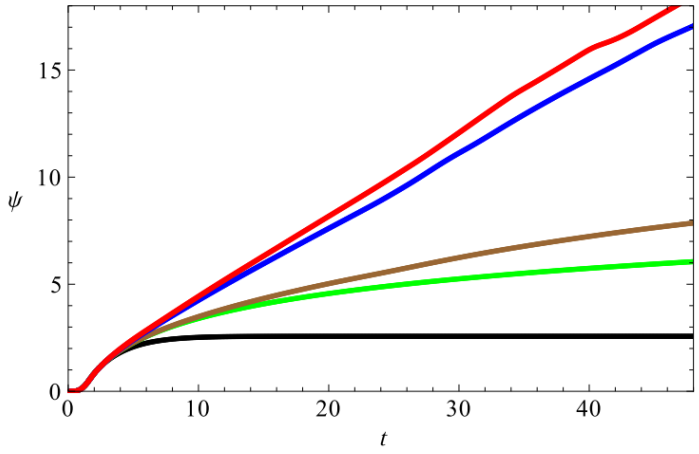
ψ
t
0
5
10
15
20
30
40

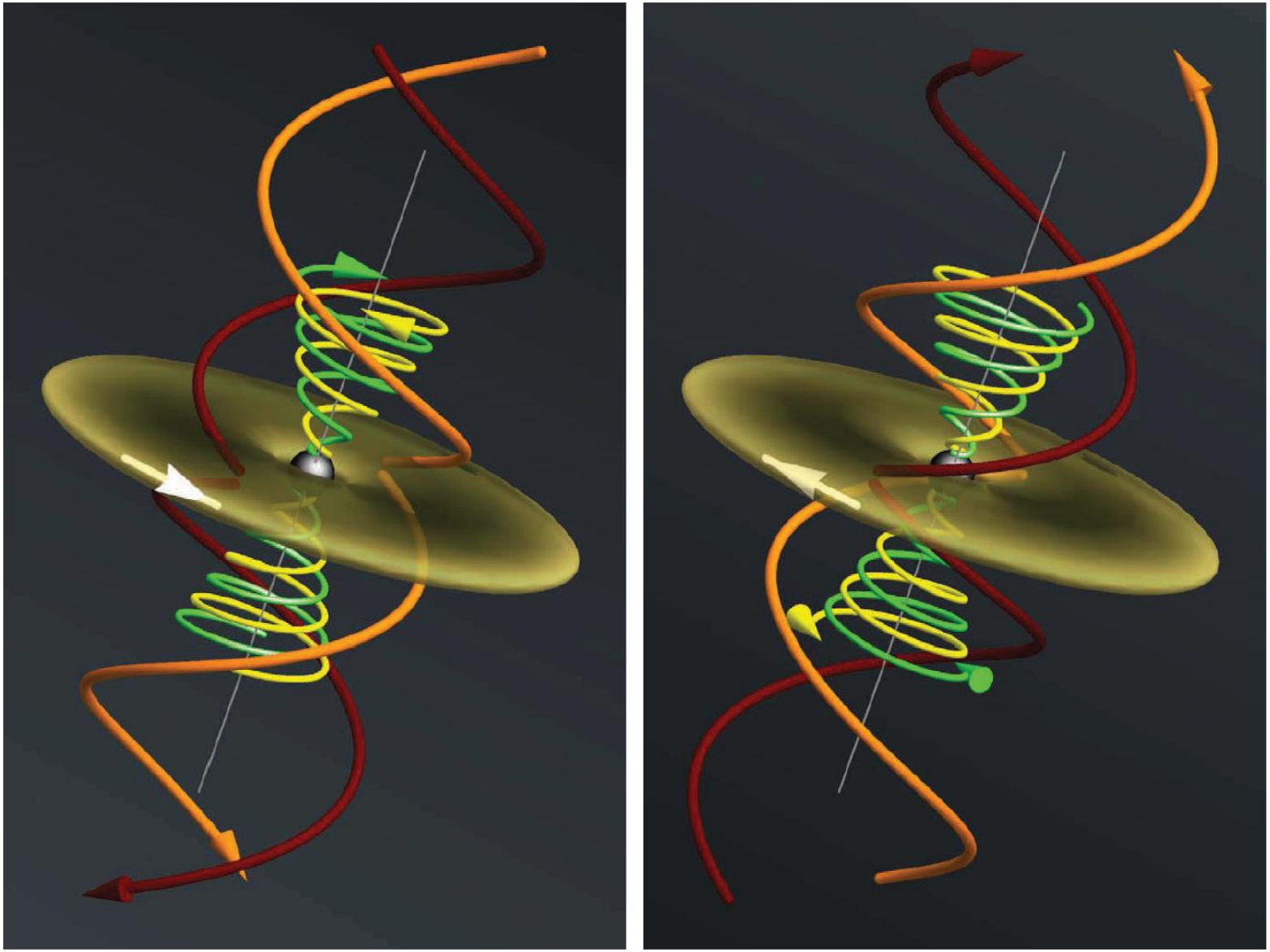

“Dominance of outflowing electric currents on decaparsec to kiloparsec scales in extragalactic jets”, Christodoulou et al. 2016

Table 1. Transverse RM gradients on decaparsec to kiloparsec scales

No. (1)	Object name (2)	z (3)	RM gradient direction (4)	Projected distance from core (pc) (5)	Instrument and frequencies (6)	References† (7)
			Firm Gradients, Significances $\geq 3\sigma$			
1	0716+714	0.127	CCW*	3–35	VLBA, 4.6-15 GHz	**Mahmud et al. (2013)**
					1.4-1.7 GHz	Healy (2013)
2	0923+392	0.695	CCW*	20	VLBA, 4.6-15 GHz	**Gabuzda et al. (2014b)**
3	5C4.114 (N)	$> 0.023^a$	CCW	> 2000	VLA, 1.4-4.9 GHz	Bonafede et al. (2010); **Gabuzda et al. (2015b)**
4	5C4.114 (S)	$> 0.023^a$	CCW	> 1500	VLA, 1.4-4.9 GHz	Bonafede et al. (2010); **Gabuzda et al. (2015b)**
5	A2142A	0.091	CCW	to $\simeq 10,000$	VLA, 4.5-8.5 GHz	Govoni et al. (2010); **this paper**
6	1652+398	0.034	CCW	20	VLBA, 8.4-1.7 GHz	**Croke et al. (2010)**
7	1749+701	0.77	CCW*	75–100	VLBA, 1.4-1.7 GHz	**Mahmud et al. (2013)**
8	3C380	0.692	CCW	70–210	VLBA, 1.4-5.0 GHz	**Gabuzda et al. (2014a)**
9	2037+511	1.687	CCW*	40	VLBA, 4.6-15 GHz	**Gabuzda et al. (2014b)**
			Tentative Gradients			
1	0156−252	2.09	CCW	4000	VLA, 1.4-8.5 GHz	Athreya et al. (1998)
2	3C120	0.033	CCW	25–80	VLBA, 1.4-1.7 GHz	Coughlan et al. (2010); this paper
3	M87	0.004	CCW	60, 960, 1400	VLA, 8-43 GHz	Algaba et al. (2013)
4	5C4.152	$\ldots^a$	CCW	15″	VLA, 4.5-8.3 GHz	Bonafede et al. (2010); this paper
5	Cen A	0.0018	CCW	130,000	ATCA, 1.3-1.5 MHz	Feain et al. (2009); this paper
6	3C303	0.141	CCW	20,000	VLA, 1.4-8.5 GHz	Kronberg et al. (2011)
7	3C465	0.0313	CCW	40,000–100,000	VLA, 4.5-8.9 GHz	Eilek & Owen (2002)

† References in bold indicate papers that present quantitative analyses of the statistical significance of the corresponding RM gradients.
*RM gradients in the CW direction are present closer to the jet base.
[a] Exact redshift not available.

"Dominance of outflowing electric currents on decaparsec to kiloparsec scales in extragalactic jets", Christodoulou et al. 2016

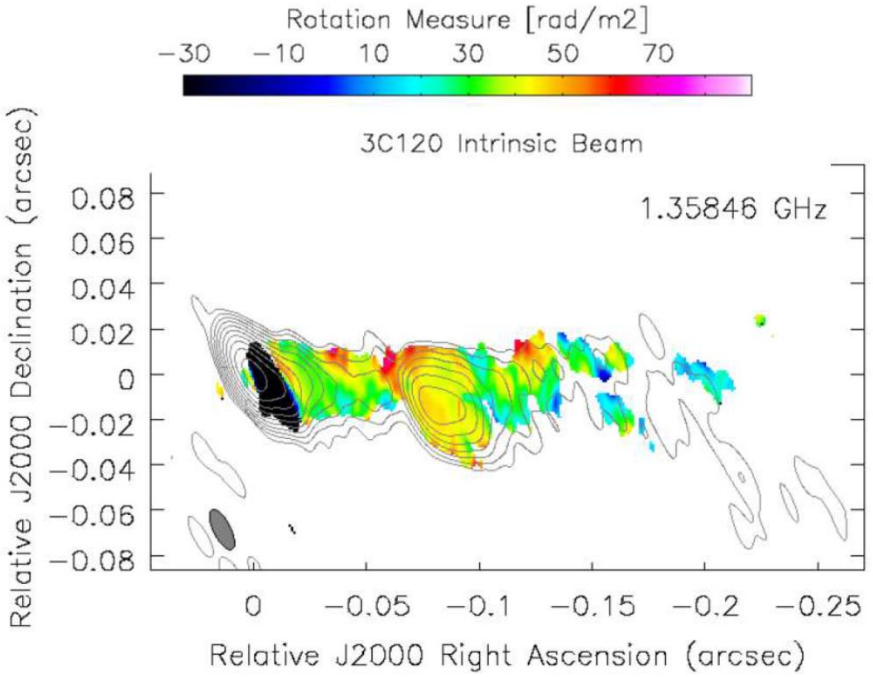

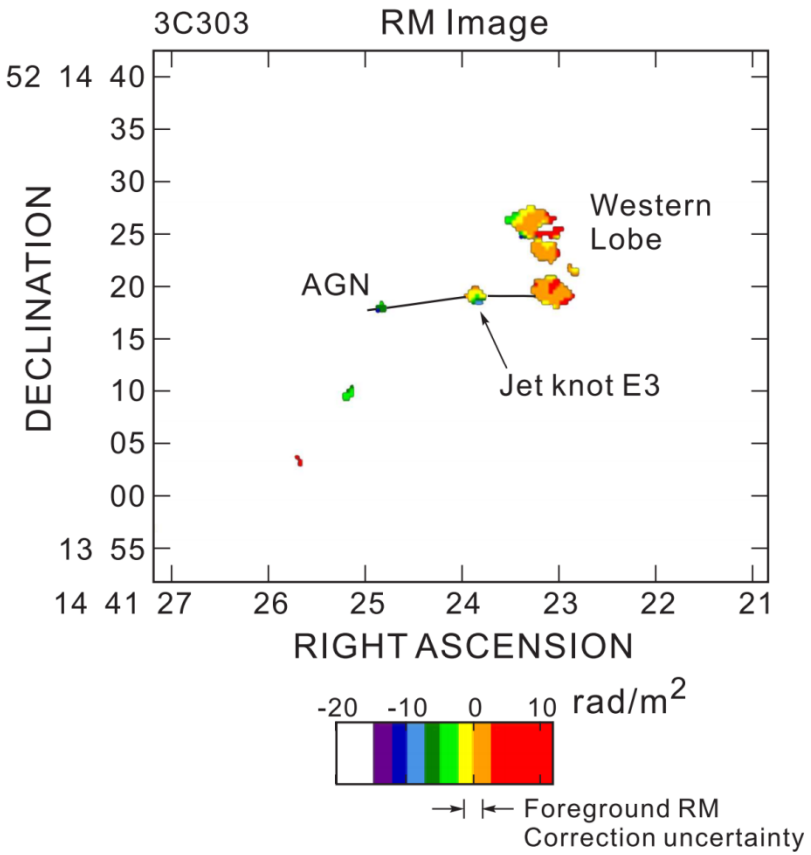

"Dominance of outflowing electric currents on decaparsec to kiloparsec scales in extragalactic jets", Christodoulou et al. 2016

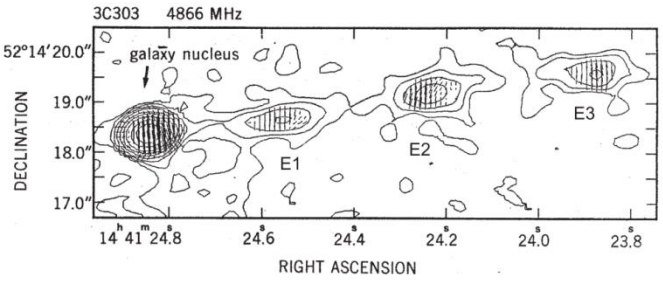

Fig. 2.— A 4.9GHz VLA image of the 3C303 jet at 0.35″ resolution showing the 3 prominent, elongated and equally spaced knots E1, E2, and E3 to the right of the stronger, variable milliarcsec-size galaxy nucleus source.

"Measurement of the electric current in a kpc-scale jet", Kronberg et al. 2011

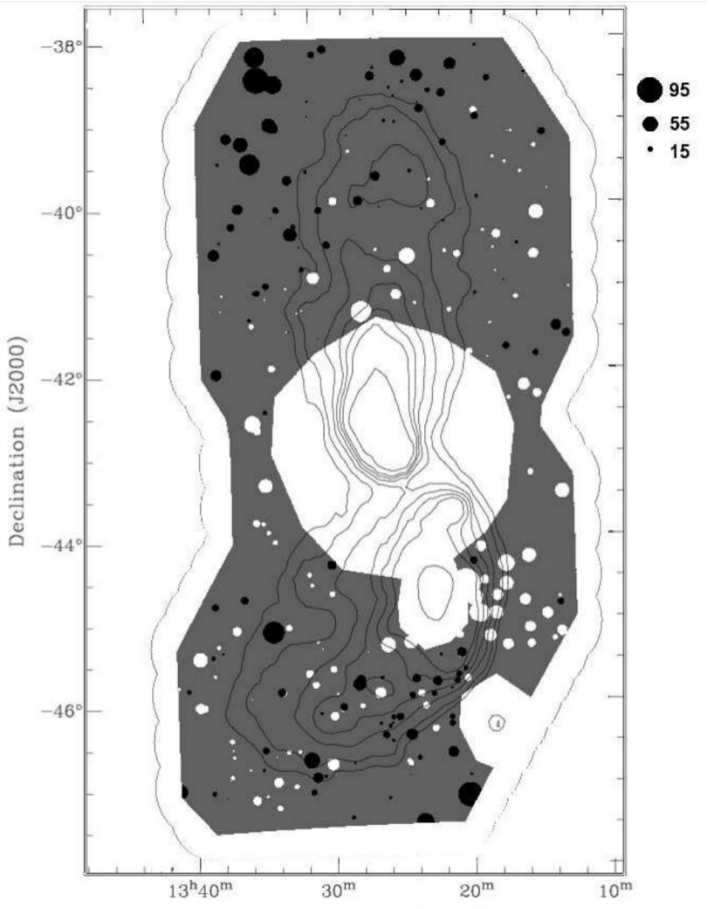

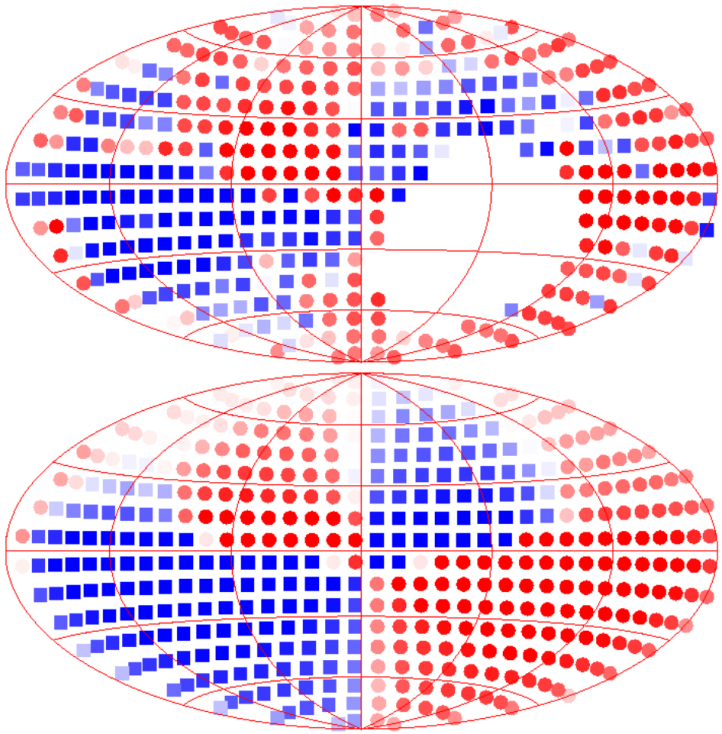

FIG. 8.— Average rotation measures in bins. Red circles (blue squares) represent positive (negative) RMs. The color intensity reflects the absolute magnitude. Top: NVSS data. Bottom: best-fit model.

"Faraday rotation structure on kiloparsec scales in the radio lobes of Centaurus A", Feain et al. 2009

"Deriving global structure of the Galactic Magnetic Field from Faraday Rotation Measures of extragalactic sources", Pshirkov et al. 2011

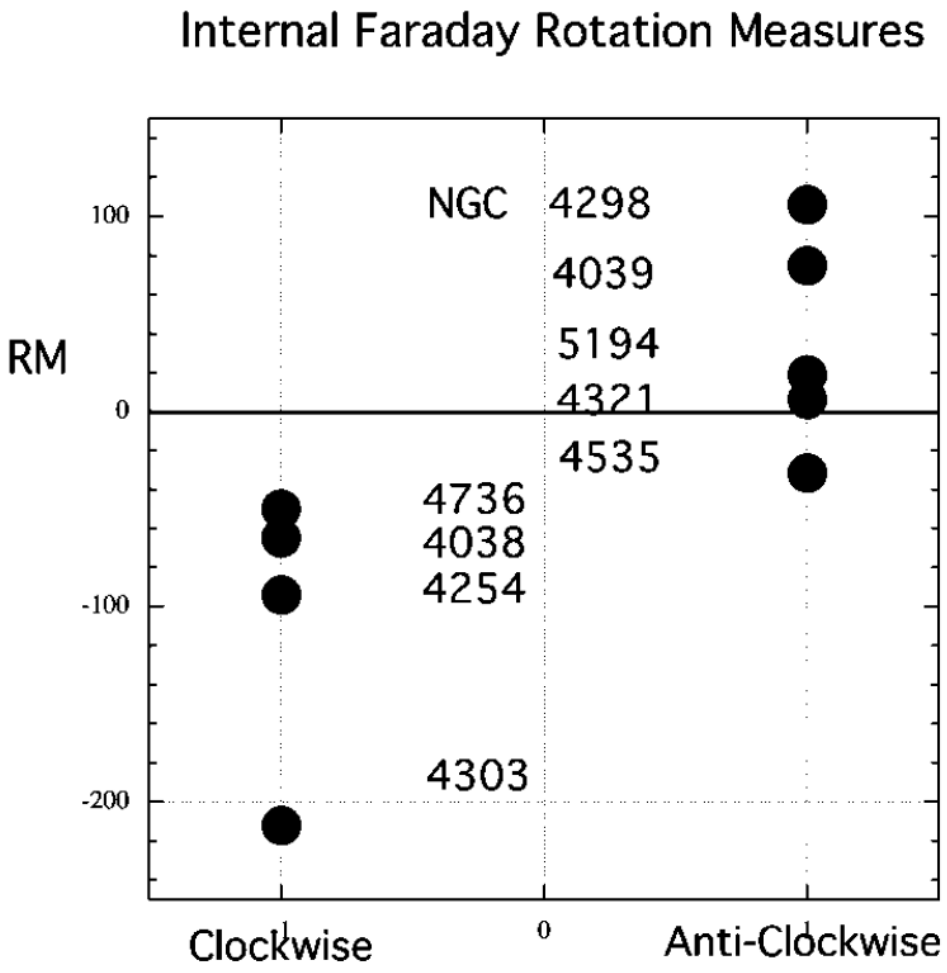

"Magnetism along spin", Lynden-Bell 2013

We know a lot about the magnetic launching of astrophysical jets…

…but we still don’t know where does the large scale ordered magnetic field come from…

…if such large scale ordered magnetic field exists…

The launching of jets from astrophysical accretion disks and black holes

Ioannis Contopoulos

2nd HELAS Summer School, Athens July 14, 2016